The Impact of Hurricane Sandy on the Shoreface and Inner Shelf of Fire Island, New York: Large Bedform Migration But Limited Erosion

John A. Goff*[1], Roger D. Flood[2], James A. Austin, Jr.[1], William C. Schwab[3], Beth Christensen[4], Cassandra M. Browne[1], Jane F. Denny[3], Wayne E. Baldwin[3]

*Corresponding Author: goff@ig.utexas.edu

[1] *Institute for Geophysics, Jackson School of Geosciences, University of Texas at Austin, Austin, TX, 78758, USA*

[2]*School of Marine and Atmospheric Sciences, Stony Brook University, Stony Brook, NY, 11794, USA*

[3]*US Geological Survey, Woods Hole, MA, 02543, USA*

[4]*Environmental Studies Program, Adelphi University, Garden City, NY, 11530, USA*

Abstract

We investigate the impact of superstorm Sandy on the lower shoreface and inner shelf offshore the barrier island system of Fire Island, NY using before-and-after surveys involving swath bathymetry, backscatter and CHIRP acoustic reflection data. As sea level rises over the long term, the shoreface and inner shelf are eroded as barrier islands migrate landward; large storms like Sandy are thought to be a primary driver of this largely evolutionary process. The "before" data were collected in 2011 by the U.S. Geological Survey as part of a long-term investigation of the Fire Island barrier system. The "after" data were collected in January, 2013, ~two months after the storm. Surprisingly, no widespread erosional event was observed. Rather, the primary impact of Sandy on the shoreface and inner shelf was to force migration of major bedforms (sand ridges and sorted bedforms) 10's of meters WSW alongshore, decreasing in migration distance with increasing water depth. Although greater in rate, this migratory behavior is no different than observations made over the 15-year span prior to the 2011 survey. Stratigraphic observations of buried, offshore-thinning fluvial channels indicate that long-term erosion of older sediments is focused in water depths ranging from the base of the shoreface (~13-16 m) to ~21 m on the inner shelf, which is coincident with the range of depth over which sand ridges and sorted bedforms migrated in response to Sandy. We hypothesize that bedform migration regulates erosion over these water depths and controls the formation of a widely observed transgressive ravinement; focusing erosion of older material occurs at the base of the stoss (upcurrent) flank of the bedforms. Secondary storm impacts include the formation of ephemeral hummocky bedforms and the deposition of a mud event layer.

Keywords: Superstorm Sandy, Sand Ridges, Sorted Bedforms, Shoreface, Inner Shelf, Ravinement

1.0 Introduction

"Superstorm" Sandy made landfall as a post-tropical cyclone, with 70-knot maximum sustained winds, near Brigantine, NJ, on October 29, 2012 (Figures 1, 2). Its sustained winds were ~25% higher, and significant wave heights ~50% higher than most other large storms over the previous 17 years (Figure 2). Its unusual shoreward trajectory and massive size created record storm surges for longer periods along the heavily populated New Jersey and New York coastlines (Figure 1; http://www.nhc.noaa.gov/data/tcr/AL182012Sandy.pdf). Infrastructure in the New York City metropolitan area was heavily damaged, and the Long Island barrier island system was both breached in places and seriously eroded (Hapke et al., 2013).

The impacts of this storm on the shoreface and inner shelf, which are permanently submerged and therefore primarily accessible only through acoustic mapping, are harder to observe. However, although the shoreface and inner shelf are neither populated nor veneered with human infrastructure, they are nevertheless critical to both people and their structures, because they are the first line of defense of barrier island systems against a naturally retreating, or "transgressing," coastline. Under rising sea level conditions, the natural condition today along most of the U.S. east coast, barrier islands will back-step (retreat landward) by erosion on the seaward side and deposition on the landward side (Bruun, 1962; Swift and Thorne, 1991; Thorne and Swift, 1991). Large storms, with consequent high waves, strong currents and above-normal tidal ranges/surges, are thought to be primary drivers of such shoreface erosion (Swift, 1968; Swift and Thorne, 1991). Such storms are also considered important contributors to landward aggradation through overwash deposition (Lentz et al., 2013), although island breaching and inlet formation/closure are also major drivers over the short term (Leatherman, 1985).

There are few observational studies of large-storm impacts on the shoreface that can help constrain the storm-driven sediment budget for any barrier system. Logistically, such studies are difficult to organize because they require rapid mobilization of survey assets as soon after the storm as possible. Some luck is also required in order to have available any recent pre-storm surveys of like kind against which post-storm data can be compared. Furthermore, comparative studies done to date have resulted in different conclusions about hurricane impacts. After Hurricane Ike in 2008, for example, Goff et al. (2014) documented a widespread "storm" event involving up to 1 m of erosion on the Bolivar Peninsula, TX, shoreface. In contrast, after Hurricane Ivan in 2004, Kraft and de Moustier (2010) found up to 1 m of deposition along the shoreface of Santa Rosa Island, FL. These examples suggest that how a storm impacts the shoreface is likely to be dependent in part on local factors, such as wave/current history, abundance of mobile sand, and shoreface/barrier morphology. Multiple before-and-after storm maps of the seafloor and shallow subsurface, as well as access to key observational data (waves, currents, sediment transport processes), are required before we can constrain physics-based models of processes driving sediment flux on the shoreface and inner shelf during storms.

A comprehensive survey of the Fire Island, NY, lower shoreface and inner shelf was conducted by the U.S. Geological Survey (USGS) in June, 2011 (Figures 1 and 2; Schwab et al., 2013; 2014), approximately a year and a half prior to Sandy. This pre-storm survey provides an important baseline for quantifying seabed changes during this time period. The same area was also surveyed by the USGS in 1996 and 1997 (Figure 2; Schwab et al., 2000), providing a longer-term rates-of-change baseline to compare against short-term (i.e., baseline + storm-induced) changes. To complement these pre-storm data sets, we mounted a collaborative post-Sandy survey in early January, 2013, aboard the R/V *Seawolf* to collect multibeam bathymetry and backscatter, CHIRP (compressed high-intensity sonar [previously radar] pulse) acoustic reflection data, and sediment grab samples offshore of part of southern Long Island. Two survey patches, "Fire Island West" (FIW) and "Fire Island East" (FIE), overlap the 2011 USGS survey (Figure 1), and are the focus of the results presented in this paper. The intervening time between 2011 and 2013 surveys also included the passage of Irene, which impacted the Mid Atlantic Bight as a tropical storm in late August, 2011 (http://www.noaa.gov/extreme2011/irene.html). Irene was a lesser storm in terms of winds and waves than Sandy (Figure 2). Its peak sustained winds were on par with more typical large storms in the region, but its significant wave heights were larger (Figure 2). Although our primary focus is on the larger storm, Irene could also have contributed to any observed "storm-induced" component of change.

The seabed offshore of Fire Island undergoes a significant change in morphology between the eastern and western ends of Fire Island (Figure 1; Schwab et al., 2000; 2013; 2014). To the west, the seabed morphology is dominated by shoreface-attached sand ridges, large (~1-6 m high, ~1-3 km wide) dune-like bedforms angled ~20°-50° to shore (acute angle to the east). To the east, shoreface-attached bedforms also exist, but they are smaller and narrower (<0.5-1.5 m high and ~0.2-1.0 km wide), angled ~60°-70° to shore (acute angle to the east), and are classified as "sorted bedforms" rather than as sand ridges (Schwab et al., 2013). This terminology refers to the pronounced segregation of grain sizes into coarse and fine sand regions, with coarser grain sizes flooring basins to stoss (upcurrent) slopes (Murray and Thieler, 2004). Schwab et al. (2000; 2013) link this change in shoreface and inner-shelf morphology to the abundance of modern marine sand; much more is available offshore of the western half of Fire Island, because sand is being transported westward from a large Pleistocene sand unit mid-island by longshore currents. Schwab et al. (2000; 2013) also note that the coastline of western Fire Island is presently stable or advancing, whereas to the east it is retreating. To explain this correlation, they hypothesize that shoreward advection of sand from the inner shelf contributes to the replenishment of shoreface sand off western Fire Island; they further suggest that storms contribute to this process. Consequently, the 2013 western and eastern post-Sandy surveys described in this paper provide an opportunity to investigate the shoreface response to Sandy in different settings in terms of sand thickness and seabed morphology, and to explore possible linkages to coastline stability.

2.0 Methods

2.1 Multibeam bathymetry and backscatter

The post-Sandy bathymetric and backscatter data were collected in January, 2013, (Figure 2) using a hull-mounted Kongsberg EM 3000D multibeam echosounder. This system operates at 300 kHz and utilizes two transducers to image a swath that has a width up to 10 times water depth. Vessel heave, pitch, roll and heading were recorded continuously. Sound velocity profiles were collected when possible, since these profiles could only be collected during breaks in the CHIRP survey lines, which could only occur during good weather or during sampling. The operational tempo resulted in velocity profiles separated by about 2 to 24 hours. We collected full bathymetric coverage in each survey area, along with 11 (FIW) or 20 (FIE) crossing tracks. The soundings were digitally filtered, manually edited and corrected for refraction errors. Real-time kinematic (RTK) GPS fixes were used to provide vertical elevations during the survey. Ellipsoidal elevations were calculated using corrections broadcast by the

NYSNet CORS network, which were received by cell phone. RTK Elevations referenced to Vertical Datum of 1988 (NAVD88) were calculated using the ellipsoidal heights, and the geoid elevation (geoid 12a) was determined using online software provided by the National Geodetic Survey (http://ngs.noaa.gov). RTK fixes could not be calculated during times of poor cell phone signal or poor satellite geometry, so the RTK elevations, averaged over 6-minute intervals, were integrated with offset and scaled using NOAA water-level observations collected at Sandy Hook, NJ, to provide a continuous water-level curve during the survey. Backscatter data were corrected for beam pattern. Depth grids and backscatter mosaics were made at a horizontal resolution of 1 or 2 m/pixel.

A portion of FIW was surveyed in 2005 (Figure 2) by Stony Brook University (Flood and Kinney, 2005), using the same equipment that was used in 2013, although only one transducer was used in 2005. For that survey, a local water-level gauge was deployed to measure the water-level record and the depths were referenced to MLLW (mean lower low water).

The USGS used an interferometric sonar operating at a frequency of 234 kHz to collect co-located acoustic backscatter and swath bathymetry offshore of Fire Island in June, 2011 (Figure 2; Schwab et al., 2014). Vessel heave, pitch, roll and yaw (attitude) were recorded continuously, and sound velocity profiles were collected approximately every 2 hr. Soundings were recorded over swath widths ranging from 50 to 150 m, resulting in coverage of ~90% of the seafloor in the survey area. Vessel attitude and sound velocity data were used to reduce vessel motion and refraction artifacts and filters were used to remove spurious soundings. Poor sea-state conditions rendered the outer portions of the swaths unusable; these were edited out before gridding. RTK GPS height corrections, broadcast from a Continuously Operated Reference Station (CORS) at Central Islip, NY (station NYCI), were used to reference soundings to the North American

NAVD88 and remove water depth variations caused by tides. Processed soundings were used to create an interpolated bathymetric grid with a resolution of 2 m/pixel. Acoustic backscatter data were radiometrically corrected using an empirical gain normalization function and mosaicked at a resolution of 5 m/pixel.

Technical specifications on shallow water bathymetry systems typically indicate depth resolution on the order of 1 cm (e.g., http://www.geodynamicsgroup.com/mb_ss.html), indicating that very small-scale seafloor features will be well-imaged with these systems. However, biases of perhaps 10's of cm can be associated with errors in the tidal (water level) corrections, leading to systematic inaccuracies over large areas. As demonstrated in the results below, such problems are evident in the comparison of the different bathymetric data sets, thus requiring care in interpreting the differences.

2.2 CHIRP

CHIRP data were collected concurrently with the post-Sandy (2013) multibeam data, resulting in dense coverage along shore-parallel (strike) track lines. The FIW survey dimensions are ~3500 m in the strike direction and ~3500 m in the dip (cross-shore) direction, with 75 strike lines and 11 dip lines. The FIE survey dimensions are ~5000 m in the strike direction and ~2300 m in the dip direction, with 63 strike lines and 20 dip lines. We operated an Edgetech 512i towfish using a 0.7-12 kHz, 20 ms pulse. Both full-waveform and envelope records were collected; the full waveform data were found to display greater sub-seafloor clarity, which facilitated horizon detection and mapping, particularly close to the seafloor reflection (Figure 3), and are used exclusively in this analysis. Processing was conducted using Paradigm's Focus software, and included: heave filtering, tide and fish- depth corrections, secondary deconvolution (to further sharpen the waveform image), trace equalization and water column muting. Navigation was also corrected for layback of the towfish, which was towed by a boom to the side of the vessel, relative to the ship's GPS position. Seismic horizons were identified and interpreted using Landmark's DecisionSpace software. Precision in picking the two-way travel time of a reflector is ~0.1 ms, which is the approximate width of the main lobe of the deconvolved return signal. Reflections below the seafloor are observable deeper than ~0.2 ms below the seafloor reflector.

The USGS also used an Edgetech 512i to collect CHIRP seismic-reflection data offshore Fire Island in 2011 (Schwab, 2014). Data were acquired along ~2800 km of track spaced ~75 – 100 m apart in the shore-parallel direction, with shore-perpendicular tie lines spaced ~ 2 km apart. Navigation was recorded using a Differential Global Positioning System, and coordinates were also corrected for layback of the towfish. Data were acquired using a 0.25-s shot rate, a 5-ms pulse length, and a 0.5-8.0-kHz frequency sweep; only the envelope records were analyzed. SIOSEIS (http://sioseis.ucsd.edu/) seismic processing software was used to shift traces vertically to remove the effects of sea surface heave, mute water column portions of the traces, and apply time-varying gain and automatic gain control. Processed seismic-reflection data were loaded into the seismic interpretation software package Landmark SeisWorks 2D, where reflectors were identified and digitized.

Isopach maps for both CHIRP surveys were generated by differencing the two-way travel time (TWTT) values for bottom and top boundaries of the identified sedimentary unit, and then gridding and interpolating these values on a 2-m grid. Isopach values from the 2011 survey were stored in meters after conversion from TWTT using 1500 m/s. To compare with the 2013 survey, these values were converted back to TWTT using the same sound velocity. Differences between the two surveys are expressed in both TWTT and in meters, using a sound speed more appropriate to sand of 1700 m/s (e.g., Hamilton and Bachman, 1982). Vertical resolution of an isopach measurement (i.e., the difference between two reflectors) on a single ping will be ~20 cm, and resolution of the difference between two isopachs from such individual measurements is probably on the order of ~30 cm. However, the gridded difference map affords greater precision. Two factors contribute: (1) filled grid nodes are typically the average of several individual pings, and (2) broad areas of positive or negative anomalies represent the integration of many grid nodes, and thus the average over many pings. Since errors on averages scale with $1/\sqrt{N}$, where N is the number of data points averaged, and since a broad area of consistent positive or negative differences could occur over hundreds of pings, we assume that the error on such differences is on the order of just a few centimeters.

3.0 Results

3.1 Backscatter

Multibeam backscatter data for the post-Sandy FIW and FIE surveys are presented in Figures 4 and 5, respectively. The backscatter map in both cases is dominated by the primary bedforms: sand ridges within FIW and sorted bedforms within FIE. Schwab et al. (2000; 2013; 2014) suggest that both types of bedforms are, over the long term, migrating to the west or southwest, as evidenced by coarser grain sizes and higher backscatter on the stoss (northeast) flanks. We observe that the sharpest contrast between higher and lower backscatter regions occurs at the lowest points of the swales between the sand ridges or the depressions of the sorted bedforms. Traces from these contacts from the 2011 survey have been digitized and then superposed on the post-Sandy backscatter maps (Figures 4, 5). We use this comparison to measure migration distances, avoiding regions where, as discussed below, mud has accumulated broadly in the swales (Figure 4) and obscured the contact. Measured distances indicate that that both sets of bedforms have migrated to the southwest between mid-2011 and early 2013, and that the amount of migration between the two surveys decreases with increasing water depth: 40-75 m in ~15 m depth, and ~0-30 m in ~20 m depth. If we assume such movement to be spread out over the ~1.6 year span between the June, 2011 and January, 2013 surveys, this translates into rates of 25-47 m/yr in 15 m water depth and 0-19 m/yr in 20 m water depth. We can compare these rates to bedform migration measured by Schwab et al. (2013) for the 15-year period 1996-2011. They found up to 75 m of westward migration of sand ridges off western Fire Island (5 m/yr), but no discernable migration of sorted bedforms off eastern Fire Island (0 m/yr). Circumstantially, therefore, we can attribute the higher rates of migration between the 2011 and 2013 surveys primarily to Superstorm Sandy, and perhaps secondarily to Tropical Storm Irene, as this period is not otherwise distinguishable from the previous 15 years in terms of wind and wave conditions (Figure 2). We conclude that the cyclonic storms have had a measureable, significant effect on the shoreface and inner shelf in terms of moving sand ridges and sorted bedforms beyond what might be considered longer-term, average rates of migration.

We found low backscatter values within portions of the swales and depressions in the post-Sandy data (Figures 4, 5); these were not present in earlier data sets, including the 2011 or 1996 data sets of Schwab et al. (2000; 2013), or the 2005 data set of Flood and Kinney (2005). Several grab samples taken during the FIE and FIW surveys recovered very soft, runny ("goopy") mud, of variable thickness (0 to >10 cm), overlying medium-to-fine sand (Figure 4, inset). Such muds were not observed in pre-Sandy samples. We infer that the low backscatter anomalies in the post-Sandy multibeam data are significant accumulations of such mud within topographic lows. Heavy metals were also detected within the muds (Christensen et al., 2013).

3.2 Bathymetry

Multibeam bathymetry data from the post-Sandy FIW and FIE surveys are displayed in Figures 6 and 7, respectively. Comparisons of the grids derived from the post-Sandy (2013) and pre-Sandy (2011) surveys shows an average offset of 0.15 m for FIW (2013 deeper) and 0.06 m for FIE (2013 deeper), and that the standard deviation between the surveys is 0.15 m for both surveys. While some of the depth difference between the two surveys may be related to elevation changes related to sediment movement during Sandy, the pattern of differences exhibits along-track striping suggesting that there are some systematic errors in the water-level corrections applied to the 2013 depth data.

The offset between MLLW and NAVD88 at this site is 0.73 m (NOS VDatum program. http:// http://vdatum.noaa.gov/). After correcting for that offset, the mean difference between the USGS FIW survey and the depths reported by Flood and Kinney (2005) is 0.066 m.

Our intention was to compute a bathymetric difference map between the 2011 and post-Sandy surveys in order to use that map to characterize storm-related influences on the shoreface/inner shelf seafloor. However, the resulting product was dominated by a suspicious shore-parallel pattern; i.e., highly variable (10’s of cm) over scales spanning many swaths in the dip direction, but much less so in the strike direction. Because both bathymetric maps were composed of ~shore-parallel tracks, such a pattern could be caused by errors or inconsistencies in applying tidal corrections for one or both surveys. The apparent vertical offsets appear to vary slowly, as it takes the vessel about 0.5 hours to cross the survey in the along-shore direction, and offsets between adjacent shore-parallel tracks collected consecutively are small and consistent in the along-track direction. However, some of the adjacent tracks were collected more than one day apart, leading to larger jumps between adjacent tracks and the overall across-shore striping of the difference map. The artificial nature of the shore-parallel difference pattern will be conclusively demonstrated in Section 3.3; no evidence of a shore-parallel pattern is observed in difference maps of the modern sand isopachs. These isopachs are closely correlated with bathymetry, but are measured from an observable, rather than calculated (i.e., corrected using tidal data), vertical datum in the stratigraphy.

While there appear to be problems when comparing the bathymetric maps presently available for each area, we can utilize the presence of large anthropogenic objects that occur on the seafloor in the FIW survey area as an independent vertical reference for local bathymetric comparisons. These numerous man-made objects were deliberately sunk in the south-southwest sector of the FIW survey (Figure 6) to form artificial reefs for marine habitats (Flood and Kinney, 2005). This area was also surveyed in 2005 by Flood and Kinney (2005), using the same multibeam sonar used for the post-Sandy survey. In the northwest sector of the FIW survey, there is a single, partially-buried object of unknown origin with a scour mote around it (Figure 6, black arrow).

To utilize these objects as vertical references, we sampled profiles through them, identified in Figures 4 and 6 as FIW1 (~15-16 m water depth) and FIW2 (~20-22 m water depth). We chose the profile orientation to be parallel to the track lines from the 2011 survey to avoid gaps between the swaths that existed after data editing. Using the 2011 data as the standard, we found that the FIW1 profile from 2013 needs to be shifted upward by 5 cm in order to align the seafloor object and associated scour pit seen in both surveys (Figure 8a). In contrast, the FIW2 profile from 2013 needs to be shifted upward by 15 cm to align the three seafloor objects observed on that profile (Figure 8b). Profile FIW2 also passes though the region mapped in 2005 by Flood and Kinney (2005); that profile needs to be shifted downward by 90 cm to align the objects to the 2011 profile (Figure 8b), an offset that is in part due to the fact that the 2005 survey is referenced to MLLW and not NAVD88. The stability of the seafloor objects is demonstrated by their lack of lateral movement between all surveys.

3.2.1 FIW Bathymetry

In the shallower, FIW1 profile comparison (Figure 8a), we observe two primary seafloor changes when comparing the 2011 (pre-Sandy) and 2013 (post-Sandy) surveys:

(1) Existing bedforms have migrated to the southwest. We measure a shift in the deepest part of the swales of 50-80 m in this profile (Figure 8a), which is consistent with the measured shifts in backscatter transitions seen in Figure 4.

(2) Numerous secondary bedforms have formed, most notably over the distance range 100-500 m, on the stoss (northeast) flank of a sand ridge (Figure 8a). Secondary bedforms on stoss flanks have also observed by Dalrymple and Hoogendoorn (1997) on active sand ridges offshore of Sable Island, Canada. It is not known, however, if these features form in response to storm events.

We do not observe any indication of either large-scale erosion or deposition along profile FIW1. Instead, positive and negative depth changes of 10 to 40 cm over distances of up to 200 m appear localized by bedform migration and formation.

Profile FIW2 (Figure 8b), at greater water depth than FIW1, exhibits fewer changes between pre- and post-Sandy surveys. The 2005 and 2011 profiles are nearly identical. The most significant change observed on the 2013 profile is the accumulation of up to 50 cm of new sediment that is about 200 m wide at the base of the swale, which we attribute to soft mud deposited as a result of the storm (Figure 4). In addition, there appears to be minor accumulation (up to ~10 cm) on the southwest (lee) flank of the ridge, consistent with bedform migration to the southwest, albeit to a lesser degree.

The small-scale morphology of the FIW survey is characterized in many places by hummocky (i.e., three-dimensional) bedforms on both lee and stoss sand ridge flanks (Figure 6). Comparison with backscatter (Figure 4) indicates that some of the surface muds have accumulated in these hummocky bedform depressions. This indicates that these hummocky bedforms had become inactive before the muds were deposited. Post-Sandy bedforms of similar character (identified as "jagged, mottled topography") were also mapped by Trembanis et al. (2013) offshore of southern New Jersey in ~27 m water depth. Newly-formed, post-storm hummocky bedforms were also observed by Kraft and de Moustier (2010) offshore of Santa Rosa Island, FL, after the passage of Hurricane Ivan in 2004. This morphology has been characterized by Swift et al. (1983) as a typical seabed response to turbulent storm flows. Their three-dimensional character has been assumed to form in response to oscillatory forcing generated by large storm waves (e.g., Southard et al., 1990). Hummocky bedforms have not been observed in prior surveys of the FIW area by Flood and Kinney (2005), Schwab et al. (2000) or Schwab et al. (2013). However, hummocky bedforms have been observed in sidescan data collected in 1976 on the inner shelf east of Fire Island (Swift et al., 1983). Therefore, these bedforms appear to be ephemeral features, a conclusion supported by Trembanis et al., (2013), who found that the jagged topography degraded with time following the passage of Sandy.

3.2.2 FIE Bathymetry

Unlike the FIW survey, the FIE survey area does not include stationary seafloor objects that can be used as vertical references. Nevertheless, the analysis from the FIW survey indicates that a vertical datum error is present, and that vertical shifts need to be applied which bring the profiles from various surveys into closer alignment. To do so, and once again using the 2011 survey as the reference, we raise the FIE1 2013 profile by 20 cm (Figure 9a), and the FIE2 2013 profile by 30 cm. Unfortunately, these values are subjective, useful for visualization/profile matching but not for quantifying accumulation or erosion. However, we can use these profile comparisons to quantify lateral shifts in bedforms, which are not affected by the vertical corrections.

Profile FIE1, at ~14-15 m water depth, exhibits clear migration of bedforms, as measured by the lateral shift of their depressions, of ~40-55 m to the southwest (Figure 9a). These values are consistent with the migration observed in the backscatter data (Figure 5). We also observe a sharpening of bedform peaks and valleys from 2011 to 2013, leading to greater bedform relief in most cases and an increase in cross-sectional asymmetry. This sense of asymmetry, with steeper stoss (northeast) flanks, contrasts to that of sand ridges, which are typically symmetrical along the shoreface and evolve toward steeper lee (seaward) flanks with increasing distance from shore (Swift and Field, 1981).

Profile FIE2 (Figure 9b), at ~19-20 m water depth, also exhibits bedform migration, but only ~0-20 m, again consistent with measurements from the backscatter data (Figure 5). These bedforms are likewise asymmetric, with steeper stoss (northeast) flanks.

As in the FIW survey, hummocky bedforms are observed in the FIE bathymetry (Figure 7); these were not observed previously (Schwab et al., 2013). However, unlike FIW, there is a clear association with the sorted bedforms: hummocky bedforms occur only on their stoss (northeast) flanks.

3.3 Stratigraphy

The primary goal of our stratigraphic analysis of post-Sandy CHIRP data is to measure the thickness of the modern sand layer, so that sand thickness from 2013 can be compared to pre-storm sand thickness from 2011 (Schwab et al.,2014). Sand thickness provides a means of quantifying seabed change (albeit only for the modern sediment deposit) that is independent of bathymetric data. As demonstrated in the previous section, that calculation is unfortunately subject to errors due to uncertainties in determining a common vertical datum. The modern marine sand layer is bounded above by the seafloor (or, where it occurs, by the muddy storm deposit) and below by the seismically-interpreted transgressive ravinement (Schwab et al., 2013; 2014; Goff, 2014), a term we use to define the erosional surface formed along and across the shoreface and inner shelf during the transgression of the shoreline caused by Holocene sea-level rise (Bruun, 1962; Swift and Thorne, 1991; Thorne and Swift, 1991). This ravinement overlies either relict Pleistocene and older Coastal Plain sediments or entrained estuarine deposits developed during the last glacial period that are now generally preserved only in paleo-fluvial channels (e.g., Nordfjord et al., 2006). Critically for our goal of assessing the stratigraphic impacts of Sandy, the ravinement provides a consistent acoustically-observable reference surface for both the 2011 and 2013 CHIRP surveys, unmodified by Sandy except where the surface may have been exposed to erosion at the seafloor.

3.3.1 CHIRP Profile Interpretation

The primary stratigraphic elements observed in the CHIRP data are demonstrated in Figures 10 and 11. Figure 10 crosses a swale within the FIW survey. The interpreted post-Sandy mud deposit in this swale produces both a low-backscatter signature (Figure 4) and a weak seafloor reflection. The T horizon, which we interpret as the ravinement (the Holocene transgressive unconformity, according to Schwab et al., 2013), is a sub-horizontal surface of variable reflection character: sometimes strong and continuous, elsewhere weak and discontinuous (Figure 9a). "T" truncates a buried channel to the SW, and exhibits a ~0.5-m step up at the base of the stoss (northeast) ridge flank, intersecting what would be the seafloor without the presence of a post-Sandy mud deposit. This morphology, i.e., exposure of the ravinement on the seafloor at the base of the stoss ridge flank, has been noted by Schwab et al. (2014) for this area; similar morphology was observed by Dalrymple and Hoogendoorn (1997) for sand ridges offshore Sable Island, Canada, and by Goff (2014) for sand ridges offshore of Panama City, FL. All have concluded that, because the stoss flank is an erosional surface, the step-up at this base is indicative of progressive excavation of antecedent material associated with the migration of the sand ridge. Thus, bedform migration is associated with modification of the ravinement by erosion.

The modern marine sand layer is thinner over the FIE survey, but still widely present (Figure 11). Like the FIW sand ridges, the T horizon is commonly observed to step-up at the base of the stoss flanks of the observed sorted bedform morphology. Thus, although Fire Island sand ridges and sorted bedforms differ significantly in morphology (i.e., in terms of vertical and horizontal scales, orientations with respect to shoreline, and senses of asymmetry), their stratigraphic cross-sections appear similar (i.e., in terms of the relationship between the T horizon and the stoss slope). As noted in the previous section, the small-scale hummocky bedforms were preferentially formed by Sandy on the stoss flanks of the sorted bedforms of the FIE region. This is expressed in the CHIRP data as a disrupted seafloor reflection with numerous parabolic echoes (Figure 11). The morphology of these hummocks is not otherwise observable, because of the required smoothing to remove heave artifacts in the CHIRP reflection record.

3.3.2 FIW Isopachs

An isopach map of the modern sand deposits within the FIW survey is presented in Figure 12. Overlain bathymetric contours derived from the 2013 survey demonstrate the close correlation between sand thickness and sand ridge topography. A broad region of zero (or undetectable) sand thickness is present in the southwest part of the survey, located at the base of the stoss flank of a large sand ridge that extends west of the survey extent. Shoreward, modern sand thickens, associated with the shoreface wedge (Schwab et al., 2014), the seaward edge of which occurs at ~15-16 m water depth.

We present the difference between the 2013 and 2011 modern sand isopach maps in Figure 13. Although there is variability in isopach difference, we observe that the strongest areas of accumulation are northeast of swale axes, i.e., along the lee flanks of the sand ridges. Consistent with results from backscatter and bathymetric analyses, this result suggests a southwest migration of the sand ridges between 2011 and 2013, which could be a response to Sandy. However, a similar pattern of accumulation has been found by Schwab et al. (2014) in comparing modern sand thickness changes from 1996 to 2011, suggesting that southwest migration is also the longer term pattern. Furthermore, the average change in sand thickness expressed in the difference map is only 1.5 cm, which we do not consider significant. Such a small amount could also be explained by slight but systematic differences in methodology used for horizon picking, particularly noting that the 2011 CHIRP data were interpreted using envelope records, whereas the 2013 data were interpreted with better-resolved full-waveform records (Figure 3). Hence, we conclude that the overall change in modern marine sand volume over the FIW survey region is not resolvably different from zero.

Although backscatter data indicate the presence of surficial muds within both the FIW and FIE survey areas, only in the FIW survey is the mud accumulation thick enough to be measureable with CHIRP data (see Figure 10). Figure 14 displays those accumulation values overlain on the FIW backscatter data (Figure 4), which clearly establishes the correlation between low backscatter anomalies and the presence of “goopy” mud (see also Figure 4). We observed up to 1 m of mud on 2013 seismic records in the two largest mud accumulation regions (Figures 10 and 14).

We present an isopach map for the channel fill sediments in the FIW area, defined as the interval between the Channel Base and T horizons (Figure 10), in Figure 15. These channels were originally mapped by Foster et al. (1999). We observe clear evidence of dendritic, presumably fluvial morphology, with three channels merging into one to the south; similar systems have been mapped beneath the New Jersey shelf to the southwest (Nordfjord et al., 2006). A ~150 m-wide, 12 m-deep pit is present at the confluence of the three tributary channels; the nature of the pit is unknown, but its existence is well established, since it is observed on a dip line as well as multiple strike lines. The deeper, central channel to the south is assumed to be a trunk channel, while the channels to the north are interpreted as tributaries. The trunk channel is ~5 m thick beneath the shoreface wedge (shallower than ~15-16 m water depth; Figure 12), and then decreases seaward beneath the sand ridges, eventually becoming less defined toward the seaward edge of the survey area. Assuming that, prior to exposure to the shoreface, the channel fill was approximately uniform, this observation implies that the ravinement is actively evolving through continued erosion from the toe of the shoreface to at least ~21 m water depth. This zone of long-term erosion is coincident with the range of depths in which we observe significant bedform migration of sand ridges in response to Sandy (Figure 4).

3.3.3 FIE Isopachs

An isopach map of the modern sand thickness over the FIE survey region is presented in Figure 16. Overlain bathymetry contours again highlight the close relationship between topography and sand thickness, with the thinnest sands generally coinciding with the lower stoss (northeast) flank of sorted bedforms. The toe of the shoreface wedge is at ~13-14 m water depth over most of the survey, but shoals both to the northeast and southwest. A broader region of reduced sand thickness, elongated in the dip direction, is present in the center of the survey region. This region is coincident with a buried channel (Figure 17). Shoreward of the ~17-18 m isobath, the thinner (<1 m) modern sand layer over the buried channel is not expressed in the bathymetry, but rather in a shoaling of the T horizon over the channel. Such a phenomenon was not observed over buried channels in the FIW survey (Figure 10). Seaward of the ~17-18 m isobaths, channel fill sediments are exposed at the seabed and a bathymetric depression develops with increasing expression offshore.

Interpretation of the 2011 CHIRP data did not identify a modern sand layer within the FIE survey region, except along the shoreface wedge and over portions of a few of the thickest bedforms on the inner shelf (Schwab et al., 2013). However, that interpretation utilized only the envelope CHIRP records (waveform data were not recorded), whereas our interpretation utilized the higher quality full-waveform record (see Figure 3). Although the use of envelope data for interpretation is far more common, we find that the T horizon reflector can be identified with greater confidence, and the sediment thickness resolved with greater precision, using the waveform record, particularly when it is close to the seafloor (Figure 3). Therefore, we believe it is likely that the lack of modern sand layer observed in the 2011 data set over the FIE survey area is primarily due to an inability to resolve the T horizon reflector in the envelope records, particularly when the overlying sediment cover is very thin. As a result, we cannot resolve pre- and post-Sandy changes in modern sediment thickness in the FIE region.

A FIE isopach map for the channel fill sediments is presented in Figure 17. This isopach is dominated by a single shore-normal channel in the middle of the survey area. This may be the paleo-Carman's River, which presently outflows into Bellport Bay, just landward of eastern Fire Island. A smaller channel is also observed over a short distance to the northeast. Even more so than in the FIW region, we observe in this region a decrease in channel-fill thickness with water depth. Up to 9 m thick beneath the shoreface wedge, the main channel begins to decrease in thickness at ~12-13 m water depth, reducing to <1 m thick by ~21 m water depth. The smaller channel also loses expression by ~15 m water depth. As with the FIW channel fill isopach, we infer from these observations that erosion contributing to the evolution of the transgressive ravinement is active over water depths ranging from near the base of the shoreface wedge (which is ~2-3 m shallower at FIE than at FIW) to at least ~21 m. This zone of long-term erosion is likewise coincident with the range of depths that we observe significant migration of sorted bedforms in response to Sandy.

4.0 Discussion

4.1 Bedform Migration in Response to Storm Forcing

Our primary conclusion is that superstorm Sandy caused sand ridges and sorted bedforms along the shoreface and inner shelf off Fire Island to migrate to the southwest. The amount of migration is more than observed in prior years (Schwab et al., 2013), but otherwise fully consistent with prior observations and with expectations of southwest migration based on the lee/stoss relationship of grain size (Schwab et al., 2000; 2013; 2014). This conclusion confirms what has long been hypothesized: that shoreface-attached sand ridges on wave-dominated shelves are storm-generated bedforms (Swift and Field, 1981; Calvete et al., 2001). Either cyclonic storms or nor'easters would drive shoreface sediments to the southwest south of Long Island, in the direction of observed bedform migration. In this area, prevailing wind directions during Sandy landfall (on the New Jersey coast to the south, Figure 1 inset) were strongly from the east-northeast, which could have helped drive both longshore drift and attendant bedform migration to the southwest. The migration of the sorted bedforms in the same direction is unexpected; observations of short-term stratigraphy based on short cores over such features tend to show oscillatory movement and persistence of coarse-grained patches over many years (Goff et al., 2005; Murray and Thieler, 2004; Trembanis and Hume, 2011). Nevertheless, asymmetric morphology (Murray and Thieler, 2004) and correlation to the ravinement morphology (Figure 11) imply that such bedforms do migrate over the long term. If so, large storms may be required to move them, and Sandy was such a storm.

The migration distance observed depends on water depth: ~40-75 m at the ~15 m isobath, and ~0-30 m at ~20 m isobath, both for sand ridges (Figures 4 and 8) and sorted bedforms (Figures 5 and 9). This suggests that, over the course of many migration events, these bedforms will rotate towards more acute angles with respect to the shoreline while they are active and attached to the shoreface. This behavior is not predicted by modern theoretical models of sand ridge formation (Trowbridge, 1995; Calvete et al., 2001). However, such behavior is precisely what was predicted by Swift and Field (1981) in their kinematic model for how sand ridges form at a non-orthogonal angle to the shoreline.

4.2 Evolution of the Transgressive Ravinement

Under rising sea level conditions, the long-term behavior of a barrier island is to back-step, or transgress, through erosion of the shoreface and transfer of sediment to the back bay (Swift and Thorne, 1991; Thorne and Swift, 1991). The resulting unconformity, or ravinement, separates modern sands above from Holocene estuarine sediments or Pleistocene and older sediments below (Bruun, 1962; Swift and Thorne, 1991; McBride et al., 2004; Goff, 2014). The former are typically best preserved in paleo -river channels (e.g., Schwab et al., 2000; Nordfjord et al., 2006).

Shoreface erosion and consequent evolution of the ravinement are assumed to be driven primarily by large storms, eroding the shoreface by wave and current forcing and transporting sediment inshore via storm surges (Swift and Thorne, 1991). In stratigraphic analyses, the term “wave ravinement” is often applied to this surface to indicate its presumed erosional mechanism (Allen and Posamentier, 1993; Cattaneo and Steel, 2003). A critical component of this process is that the ravinement must, even if temporarily, be exposed at the seafloor during storms so that it can be further eroded (Swift and Thorne, 1991; Thorne and Swift, 1991). Often, however, the shoreface and inner shelf are largely covered by marine sands of variable thickness (e.g., Figures 12, 16); the storm would need first to erode this overburden in order for waves and currents to erode underlying sediments. That is what appears to have happened along the Bolivar Peninsula, TX, shoreface during Hurricane Ike (Goff et al., 2014). There, the erosional event removed ~0.5 m of modern sand and then eroded an additional ~0.5 m of sediment below the preexisting ravinement. But no such erosional event was observed along the Fire Island shoreface after Sandy; the modern sand bedforms are intact, though migrated.

A critical difference between the two settings is that the Bolivar Peninsula shoreface is very shallow compared to Fire Island, extending only to ~5-6 m water depth; the erosional event documented by Goff et al. (2014) at Bolivar Peninsula occurred in only ~4 m water depth. In contrast, the Fire Island shoreface extends to ~13-16 m water depth, and the FIE and FIW surveys did not reach shallower than ~10-12 m. Therefore, it is possible that a Sandy-driven erosional event, similar to the Ike-driven Bolivar Peninsula event, occurred in water depth shallower than we were able to map offshore of Fire Island. However, the modern shoreface sand wedge is also much thicker seaward of Fire Island than on Bolivar Peninsula. Given the trends suggested by Figures 12 and 15, the shoreface wedge will be meters thick at such shallow depths, compared with ~0.5 m or less seen along the lower Bolivar shoreface (Rodriguez et al., 2001; Goff et al., 2014). Therefore, an erosional event along the Fire Island shoreface of similar magnitude and at similar depth to that of the Bolivar shoreface would not contribute to evolution of the transgressive ravinement.

The offshore gradations observed in thickness of buried river channels seaward of Fire Island (Figures 15 and 17) imply that the ravinement evolves through progressive erosion over water depths ranging from near the base of the shoreface to the ~21 m isobath. Sand ridges and sorted bedforms are also observed to have migrated along-shore in response to Sandy over this same depth range. Furthermore, exposure of the ravinement at the lower stoss flanks of these bedforms, and the stepped morphology of the ravinement at this location, indicate that sand ridge and sorted bedform migration contributes to the erosion of sediments below the ravinement, and the transference of those sediments to the modern marine sand layer (Dalrymple and Hoogendoorn, 1997; Schwab et al., 2014; Goff, 2014). Given that we observe no other significant mechanism of erosion over these water depths in response to Sandy, we hypothesize that bedform migration is a primary mechanism for evolving the transgressive ravinement along this shoreface and inner shelf. Goff (2014) has also suggested bedform migration as a primary driver for shoreface erosion and ravinement evolution, based on stratigraphic analysis of the inner shelf offshore of Panama City, FL; he has suggested the term “sand ridge ravinement” as an alternative to “wave ravinement” to describe this surface, where it is appropriate to do so.

The T horizon reflector appears to be continuous across the base of the shoreface (Schwab et al., 2013). However, if erosion contributing to the transgressive ravinement is primarily active seaward of the lower shoreface, then the nature of the reflector beneath the main part of the shoreface wedge is called into question. Under western Fire Island, it is possible that westward or offshore progradation of the barrier island has buried a previous erosional surface (Schwab et al., 2013). However, that is not the case over eastern Fire Island. Therefore, we must postulate another mechanism responsible for formation of the T reflector shoreward of the wedge. That mechanism must occur in an estuarine setting, since the horizon beneath the shoreface wedge has not yet been exposed to marine conditions. Two possibilities exist: (1) “T” is a tidal ravinement (Allen and Posamentier, 1993), or (2) “T” in this region represents a depositional boundary associated with overwashed shoreface and barrier sands over estuarine muds. In either case, the true transgressive ravinement merges with this surface by deepening its expression through marine (and perhaps primarily storm-induced) erosion.

4.3 Implications for Shoreline Stability Hypothesis

Schwab et al. (2013) have noted that the coastline along the western half of Fire Island is either stable or advancing, while the eastern half is retreating. They have correlated this observation with the change in morphology and modern sand thickness along the shoreface and inner shelf, and hypothesized that modern marine sands are replenishing the western Fire Island shoreface. A central prediction of this hypothesis is that modern sand is being advected from the inner shelf sand ridges and eroded Pleistocene sediments to the shoreface (Schwab et al., 2013). However, migration of the largest bedforms (sand ridges and sorted bedforms) is not a viable mechanism for landward advection, since the observed migration of sand ridges, both long-term (Schwab et al., 2013; 2014) and short-term (Figures 4, 8), is along-shore to offshore in a generally west-southwest to southwest direction. This transport direction is consistent with cyclonic storms like Sandy (which landed to the south of the study area) and nor'easters. However, sou'westers, a predominant wind direction in this part of the world during spring-fall months, will reverse the primary current direction so that, at least temporarily, finer-grained southwest flanks of sand ridges will become the stoss side of the bedform, and thus highly susceptible to erosion. Transport of sand from the sand ridges to the shoreface may occur during these events. Flood and Kinney (2005) have also found that smaller sand-wave bedforms in the FIW region migrated, at least in part, in a shoreward direction.

While landward transport of sand from the sand ridges to the shoreface may provide a positive feedback for shoreline stability, erosion at the base of the shoreface wedge and inner shelf may provide a negative one. As evidenced by the reduction in buried channel thickness (Figures 15 and 17), the FIW area has undergone ~3-4 m of erosion over these water depths, whereas the FIE area has undergone ~7-8 m of erosion. The observed difference could be associated with differences in bedforms, e.g., the more numerous, though smaller sorted bedforms in the FIE area facilitate erosion of underlying material during migration, whereas the wider, thicker sand ridges in FIW do more to insulate the lower shoreface and inner shelf from such erosion. Alternatively, relict Pleistocene sediments beneath eastern Fire Island may be more erodible than those beneath western Fire Island, although there is no evidence to suggest it (Schwab et al., 2013). Whatever the cause, enhanced erosion at the base of the shoreface would likely steepen the shoreface wedge at a higher rate, and help to drive coastline retreat.

4.4 Secondary Impacts: Hummocky Bedforms and Surficial Mud Layer

In addition to the migration of large bedforms, we document two other impacts of Sandy on the shoreface and inner shelf: small-scale hummocky bedforms and a surficial mud deposit of highly variable thickness.

Hummocky, cross-stratified bedforms are an important stratigraphic marker in outcrop studies (Swift et al., 1983; Duke, 1985). Presumed to form under oscillatory forcing by storm waves (Southard et al., 1990; Green et al., 2004; Trembanis et al., 2004), they are used to infer shallow-water, storm-dominated shelf paleo-conditions. However, there are few studies that link hummocky bedforms to formative mechanisms, either observationally or through modeling (Southard et al., 1990). Our surveys provide an opportunity to further the understanding of these bedforms. A follow-up study is being conducted to quantify hummocky bedforms statistically, to understand their distribution in relation to large-scale bedforms, water depth and sediment texture, and to relate these observations to storm history of waves and currents (Arora et al., 2014). The lack of any prior observations of hummocky bedforms in the FIW and FIE regions

(Schwab et al., 2000, 2013; Flood and Kinney, 2005) suggests that they are ephemeral, and will disappear once more ambient hydrodynamic conditions are established. Trembanis et al. (2013), for example, observed a gradual moderation of storm-generated "jagged mottled topography" (which we equate with hummocky morphology in our study) in multiple post-Sandy surveys offshore of Brigantine, New Jersey.

The post-Sandy mud layer was concentrated in whatever accommodation space was available, most notably in the ridge swales and sorted bedform depressions, but also in smaller areas such as scour pits and even the lower parts of the hummocky bedforms (Figures 4, 6, and 14). The presence of heavy metals in these sediments suggests that they were derived at least in part from contaminated estuarine deposits behind the barrier island, which was breached by Sandy (Christensen et al., 2013). If so, deposition of these sediments on the inner shelf attests to the importance of an ebbing storm surge in transporting back-barrier sediments offshore (Goff et al., 2010). Fine-grained sediments could also have been derived from estuarine material residing in the seismically observed paleo-channels and exposed at the seafloor on the inner shelf (Schwab et al., 2013), introduced to the area by the Hudson River during Sandy or earlier storms, or stripped from shelf sands during extreme resuspension events. Additional work will be required to ascertain provenance conclusively. As with the hummocky bedforms, localized muddy deposits have not been observed in previous surveys of this region, and are likely to be ephemeral, as subsequent storms will presumably re-entrain the mud and transport it out of the survey area, or burrowing animals will mix it into underlying sandy sediments. Further investigation of these muds is underway (Christensen et al., 2014).

5.0 Conclusions

Over the long term, barrier islands migrate landward in response sea level rise by erosion on the seaward side and deposition in the bay side; large storms are assumed to be primary drivers of this process (Swift and Thorne, 1991; Thorne and Swift, 1991). The stability of a barrier island is linked to the extent of seaward erosion which, along modern shores, excavates antecedent sediments, and forms an erosional unconformity, or ravinement, generally underlying a modern marine sand layer. The submarine impact of a storm on the barrier system can be measured by the extent to which such a punctuated, catastrophic event erodes and deepens the ravinement.

Our results demonstrate that, although superstorm Sandy was damaging to communities and infrastructure on land, its erosional impact on the sediments of the shoreface and inner shelf was limited in study areas on the western south shore of Long Island. The modern marine sand layer that mantles both the shoreface and inner shelf remained largely intact following Sandy. Major bedforms of the modern marine sand layer, sand ridges and sorted bedforms, migrated 10’s of meters in response to the storm with consequent vertical changes of 10’s of cm, but otherwise were not significantly altered in terms of their overall morphology. The only locations where we can document erosion at the ravinement are along the lower stoss (upcurrent) flanks of these bedforms, where the ravinement is often exposed at, or is very close to, the seafloor. A frequently-observed step-up in the topography of the ravinement at this location means that the surface erodes, and excavated Pleistocene glacio-fluvial material (Schwab et al., 2013) is transferred to the modern marine sand layer by deposition on the lee side, as the bedforms migrate. Therefore, sand ridges and sorted bedforms appear to act as regulators of storm-forced erosion of material beneath the modern marine sand layer. Although these bedforms are derived from eroded material, if thick enough the modern sand layer can inhibit, if not entirely prevent, continued erosion of older sediments.

Based on observations of seaward-thinning buried fluvial channels below the ravinement, erosion at the ravinement extends from the lowermost base of the shoreface out to at least ~21 m water depth on the inner shelf. This range of depths is coincident with the area where we observe the greatest migration of sand ridges and sorted bedforms in response to Sandy. Absent any other evident erosion mechanism, we hypothesize that migration of these bedforms constitutes a primary mechanism for evolution of the transgressive ravinement, and that the undulatory morphology of the ravinement underlying the sand ridges is a consequence of such evolution.

Schwab et al. (2000, 2013) have noted that the coastline along western Fire Island is either advancing or stable, whereas along the eastern half of the island it is retreating; they have correlated this observation to observed changes in offshore morphology and modern sand availability along the shoreface and inner shelf. They have further hypothesized that modern sand from the inner shelf is being transported to the shoreface, thereby stabilizing the coastline. However, the sediment transport direction indicated by the observed post-Sandy migration of bedforms is either along-shore or along- and off-shore. This migration direction is consistent with forcing by either cyclonic storms or nor'easters. During sou'westers, however, the flow direction will reverse, exposing finer-grained sands on eroding stoss flanks, which face seaward. Shoreward transport may occur during these events. It is also possible that coastline retreat along the eastern half of Fire Island is related to a greater degree of inner shelf erosion in that area, evidenced by the seaward-thinning of buried river channels, and consequent steepening of the shoreface wedge.

Finally, we also observed secondary storm impacts, including the formation of small-scale hummocky bedforms and the deposition of an event layer of mud derived from back-barrier bay sediments. We expect both to be ephemeral, as ambient conditions smooth out hummocks and future storms re-erode muddy deposits and transport them elsewhere. Follow-up studies will focus on both sets of features.

Acknowledgements

We thank the captain and crew of the *R/V Seawolf*, owned and operated by Stony Brook University, for their tireless work and dedication. S. Saustrup at UTIG helped to process the CHIRP profiles. This work was funded primarily by a rapid response grant from the Jackson School of Geosciences, The University of Texas/Austin. UTIG Contribution Number ----.

References

Allen, G.P., and Posamentier, H.W., 1993. Sequence stratigraphy and facies model of an incised valley fill: the Gironde Estuary, France. J. Sed. Petr. 63, 378-391.

Arora, K., Goff, J.A., Wood, L., and Flood, R.D., 2014. Statistical Analysis of Small-Scale Bedforms Formed by Hurricane Sandy Offshore Fire Island, New York, submitted to 2014 Fall Meeting, AGU.

Bruun, P., 1962. Sea-level rise as a cause of shore erosion. J. Waterways Harbors Divisions 88, 117-130.

Calvete, D., Falques, A., De Swart, H.E., Walgreen, M., 2001. Modelling the formation of shoreface-connected sand ridges on storm-dominated inner shelves. J. Fluid Mech. 441, 169-193.

Cattaneo, A., Steel, R.J., 2003. Transgressive deposits: a review of their variability. Earth-Sci. Rev. 62, 187-228.

Christensen, B.A., Goff, J.A., Austin, J.A., Browne, C.M., Duzgoren-Aydin, N.S., Flood, R.D., McHugh, C.M., Dutton, J., Hosseini, P., and Brownawell, B., 2013. Soupy surface muds: A probable Sandy storm horizon with a potential source fingerprint. Abstract OS31A-1697 presented at the 2013 Fall Meeting, AGU.

Christensen, B.A., Goff, J.A., Flood, R.D., Austin, J.A., Browne, C.M., and Saustrup, S., 2014. Hurricane Sandy's Impact on Coastal Sedimentation on Long Island's South Shore: Results from a 2013 Rapid Response Study. Abstract OS23C-1231 presented at the 2014 Fall Meeting, AGU

Dalrymple, R.W., Hoogendoorn, E.L., 1997. Erosion and deposition on migrating shoreface-attached ridges, Sable Island, eastern Canada. Geosci. Canada 24, 25-36.

Duke, W.L., 1985. Hummocky cross-stratification, tropical hurricanes, and intense winter storms. Sedimentology 32, 167-194.

Flood, R.D. and J. Kinney, 2005. Temporal variability in inner shelf morphology shown by repeat multibeam surveys off Long Island. Abstract OS23A-1530 presented at the 2005 Fall Meeting, AGU.

Foster, D.S., Swift, B.A., Schwab, W.C., 1999. Stratigraphic framework maps of the nearshore area of southern Long Island from Fire Island to Montauk Point, New York. U.S. Geological Survey Open-File Report 99-559, http://pubs.usgs.gov/of/1999/of99-559/.

Goff, J.A., 2014. Seismic and core investigation of Panama City, Florida, reveals sand ridge influence on formation of the shoreface ravinement. Cont. Shelf Res. 88, 34-46.

Goff, J. A., Mayer, L.A., Traykovski, P., Buynevich, I., Wilkens, R., Raymond, R., Glang, G., Evans, R.L., Olson, H., and Jenkins, C., 2005. Detailed investigation of sorted bedforms, or "rippled scour depressions," within the Martha's Vineyard Coastal Observatory, Massachusetts. Cont. Shelf Res. 25, 461-484.

Goff, J.A., Allison, M.A., and Gullick, S.P.S, 2010. Offshore transport of sediment during cyclonic storms: Hurricane Ike (2008), Texas Gulf Coast, USA. Geology 38, 351-354.

Goff, J.A., Allison, M.A., Gulick, S.P.S., Reece, R., Davis, M., Duncan, D., and Saustrup, S., 2014. Shoreface ravinement evolution tracked by repeat geophysical surveys following Hurricane Ike, Bolivar Peninsula, Texas, 2008-2013. Geophysics, submitted (revised).

Green, M.O., Vincent, C.E., and Trembanis, A.C., 2004. Suspension of coarse and fine sand on a wave-dominated shoreface, with implications for the development of rippled scour depressions. Cont. Shelf Res. 24, 317-335.

Hapke, C.J., H.F. Stockdon, W.C. Schwab and M.K. Foley, 2013. Changing the paradigm of response to coastal storms. Eos Trans. AGU 94, 189-190.

Hamilton, E.L., and Bachman, R.T., 1982. Sound velocity and related properties of marine sediments. J. Acous. Soc. Am. 72, 1891-1904.

Kraft, B.J., and de Moustier, C., 2010. Detailed bathymetric surveys offshore Santa Rosa Island, FL: Before and after Hurricane Ivan (September 1, 2004). IEEE J. Ocean. Eng. 35, 453-470.

Leatherman, S.P., 1985. Geomorphic and stratigraphic analyses of Fire Island, New York. Mar. Geol. 63, 173-195.

Lentz, E.E., Hapke, C.J., Stockdon, H.F., and Hehre, R.E., 2013. Improved understanding of near-term barrier island evolution through multi-decadal assessment of morphologic change. Mar. Geol. 337, 125-139.

McBride, R.A., Moslow, T.F., Roberts, H.H., Diecchio, R.J., 2004. Late Quaternary geology of the northeast Gulf of Mexico shelf: sedimentology, depositional history and ancient analogs of a major shelf sand sheet of the modern transgressive systems tract, in: Anderson, J.B., Fillon, F.H. (Eds.), Late Quaternary Stratigraphic Evolution of the Northern Gulf of Mexico Margin, SEPM Special Publication No. 79, Tulsa, OK, pp. 55–83.

McCallum, B.E., Wicklein, S.M., Reiser, R.G., Busciolano, R., Morrison, J., Verdi, R.J., Painter, J.A., Frantz, E.R., and Gotvald, A.J., 2013. Monitoring storm tide and flooding from Hurricane Sandy along the Atlantic coast of the United States, October 2012: U.S. Geological Survey Open-File Report 2013–1043, 42 p., http://pubs.usgs.gov/of/2013/1043/.

Murray, A.B., and Thieler, E.R., 2004. A new hypothesis and exploratory model for the formation of large-scale inner-shelf sediment sorting and “rippled scour depressions”. Cont. Shelf Res. 24, 295-315.

Nordfjord, S., Goff, J.A., Austin, J.A. Jr., Gulick, S.P.S., 2006. Seismic facies of incised valley-fills, New Jersey continental shelf: Implications for erosion and preservation processes acting during late Pleistocene/Holocene transgression. J. Sed. Res. 76, 1284-1303.

Rodriguez, A.B., M.L. Fassell, and J.B. Anderson, 2001. Variations in shoreface progradation and ravinement along the Texas coast, Gulf of Mexico. Sedimentology 48, 837-853.

Schwab, W.C., Thieler, E.R., Allen, J.R., Foster, D.S., Swift, B.A., and Denny, J.F., 2000. Influence of inner-continental shelf geologic framework on the evolution and behavior of the barrier-island system between Fire Island Inlet and Shinnecock Inlet, Long Island, New York. J. Coast. Res. 16, 408-422.

Schwab, W.C., W.E. Baldwin, C.J. Hapke, E.E. Lentz, P.T. Gayes, J.F Denny, J.H List and J.C. Warner, 2013. Geologic evidence for onshore sediment transport from the inner continental shelf: Fire Island, New York. J. Coast. Res. 29, 526-544.

Schwab, W.C., Baldwin, W.E., Denny, J.F., Hapke, C.J., Gayes, J.T., List, J.H., and Warner, J.C., 2014. Modification of the Quaternary stratigraphic framework of the inner-continental shelf by Holocene marine transgression: An example offshore of Fire Island, New York. Mar. Geol. 355, 346-360.

Southard, J.B., Lambie, J.M., Federico, D.C., Pile, H.T., and Weidman, C.R., 1990. Experiments on bed configurations in fine sands under bidirectional purely oscillatory flow, and the origin of hummocky cross-stratification. J. Sed. Petr. 60, 1-17.

Swift, D.J.P., 1968. Coastal erosion and transgressive stratigraphy. J. Geol. 75, 444-456.

Swift, D.J.P., and Field, M.E., 1981. Evolusion of a classic sand ridge field: maryland sector, North American inner shelf. Sedimentology 28, 461-482.

Swift, D.J.P., Thorne, J.A., 1991. Sedimentation on continental margins, I: a general model for shelf sedimentation, in Swift, D.J.P. (Ed.), Shelf Sand and Sandstone Bodies: Geometry, Facies and Sequence Stratigraphy, Special Publications of the International Association of Sedimentologists, vol. 14, Wiley, Hoboken, New Jersey, pp.3-31.

Swift, D.J.P., Figueiredo, A.G., Freeland, G.L., and Oertel, G.F., 1983. Hummocky cross-stratification and megaripples: A geologic double standard? J. Sed. Petr. 3, 1295-1317.

Thorne, J.A., Swift, D.J.P., 1991. Sedimentation on continental margins, VI: a regime model for depositional sequences, their component system tracts, and bounding surfaces, in Swift, D.J.P. (Ed.), Shelf Sand and Sandstone Bodies: Geometry, Facies and Sequence Stratigraphy, Special Publications of the International Association of Sedimentologists, vol. 14, Wiley, Hoboken, New Jersey, pp. 189-255.

Trembanis, A.C., and Hume, T.M., 2011. Sorted bedforms on the inner shelf off northeastern New Zealand: spatiotemporal relationships and potential paleo-environmental implications. Geo-Mar. Lett. 31, 203-214.

Trembanis, A.C., Wright, L.D., Friedrichs, C.T., Green, M.O., and Hume, T., 2004. The effects of spatially complex inner shelf roughness on boundary layer turbulence and current and wave friction: Tairua embayment, New Zealand. Cont. Shelf. Res. 24, 1549-1571.

Trembanis, A., DuVal, C., Beaudoin, J., Schmidt, V., Miller, D., and Mayer, L., 2013. A detailed signature from Hurricane Sandy revealed in bedforms and scour. Geoch. Geophys. Geosyst. 14, doi: 10.1002/ggge.20260.

Trowbridge, J.H., 1995. A mechanism for the formation and maintenance of shore-oblique sand ridges on storm-dominated shelves. J. Geophys. Res. 100, 16,071-16,086.

Figure Captions

Figure 1. (a) Backscatter and (b) swath bathymetry data collected by the USGS in 2011 (Schwab et al., 2013), providing a basis for pre- and post-Sandy comparisons. Boxes indicate locations of post-Sandy Fire Island West (FIW) and Fire Island East (FIE) surveys. The FIW survey sampled sand ridges, whereas the FIE survey sampled a sorted bedform morphology. Inset shows location on south shore of Long Island, the track of Sandy, location of buoy 44025 used for data plotted in Figure 2, and sampled storm tide elevations above normal along the coast in meters (USGS Portal for Hurricane Response, http://54.243.149.253/; McCallum et al., 2013).

Figure 2. Sustained wind speeds (a) and significant wave heights (b) from 1996 through 2013 at NOAA buoy 44025 (http://www.ndbc.noaa.gov/station_page.php?station=44025) anchored offshore of Fire Island at ~40 m water depth (location shown in Figure 1 inset). The timing of the surveys discussed in this paper are identified. Sandy attained sustained wind speeds of 25.1 m/s and significant wave heights of 9.65 m. These values are ~25% and ~50% higher, respectively, than most other strong storms during this time period. Wave heights (b) for Tropical Storm Irene represent the lone exception. Irene impacted the Mid Atlantic Bight in late August of 2011, after the 2011 survey and therefore within the same time window between surveys as Sandy. Buoy 44025 was not operational during the passage of Irene. Peak wind and wave values for Irene are indicate from nearby buoy 44065.

Figure 3. Example of full waveform (top) and envelope (bottom) records of CHIRP data in the FIE survey region. A shallow sub-seafloor reflection (arrows) can be confidently identified in

the full waveform record, but not in the envelope record. Consequently, the former were used for interpretation and mapping of sub-seafloor horizons.

Figure 4. Post-Sandy multibeam backscatter compilation within Fire Island West (FIW) survey area; brighter shades indicate higher backscatter. See Figure 1 for location; coordinates in UTM zone 18N. Yellow lines indicate bright/dark transitions observed in 2011 backscatter data (Schwab et al., 2013). Tick marks with values indicate estimated migration of that boundary in meters between the two surveys. Inset photo shows goopy mud overlying medium sand sampled from a sediment grab in this region.

Figure 5. Post-Sandy multibeam backscatter compilation within Fire Island East (FIE) survey area; brighter shades indicate higher backscatter. See Figure 1 for location; coordinates in UTM zone 18N. Yellow lines indicate bright/dark transitions observed in 2011 backscatter data (Schwab et al., 2013). Tick marks and values indicate estimated migration of that boundary in meters between the two surveys.

Figure 6. Post-Sandy multibeam bathymetry for Fire Island West (FIW) survey, artificially illuminated from the N. “H” highlights numerous fields of hummocky bedforms observed in the data. See Figure 1 for location; coordinates in UTM zone 18N. The black arrow indicates an object on seafloor seen on sampled profile FIW1, and the yellow arrows indicate objects on profile FIW2 (Figure 8). Numerous other artificial objects, a few of which are identified with white arrows, are observed in the south-southeast quadrant of the survey. Location is also shown for the CHIRP data shown in Figure 10.

Figure 7. Post-Sandy multibeam bathymetry for Fire Island East (FIE) survey, artificially illuminated from the N. “H” highlights numerous fields of hummocky bedforms observed in the data. See Figure 1 for location; coordinates in UTM zone 18N. Profiles FIE1 and FIE2 are shown in Figure 9. Location is also shown for the CHIRP data shown in Figure 11.

Figure 8. Comparison of bathymetry along profiles (a) FIW1 and (b) FIW2 (Figures 4 and 6) for data collected in 2005, 2011 and 2013 (post- Sandy). Profiles from 2005 and 2013 were shifted to the 2011 profile vertical reference provided by emplaced seafloor objects; dotted lines of same color indicate position prior to shifting. Vertical lines and values in (a) indicate migrations of swales in meters between the 2011 and 2013 surveys. Such migration is consistently to the southwest.

Figure 9. Comparison of bathymetry along profiles (a) FIE1 and (b) FIE2 (Figures 5 and 7) for data collected in 2011 (pre-Sandy) and 2013 (post-Sandy). Profiles from 2013 were shifted to correspond to the approximate vertical position of the 2011 profiles, but without fixed seafloor objects to provide an objective reference; dotted lines of same color indicate position prior to shifting. Vertical lines and values indicate migration of swales in meters between the 2011 and 2013 surveys. Systematic southwest migration of bedforms is again indicated, as is true for the area of the FIW survey (Figure 8a).

Figure 10. Uninterpreted (top) and interpreted (bottom) CHIRP acoustic reflection profile within the Fire Island West (FIW) survey area, illustrating the primary reflection horizons and

interpreted stratigraphic units. “T” refers to the transgressive ravinement discussed in the text. Location shown in Figures 4 and 6. Depth conversion assumes a velocity of 1700 m/s in sand.

Figure 11. Uninterpreted (top) and interpreted (bottom) CHIRP acoustic reflection profile within the Fire Island East (FIE) survey area, illustrating the primary reflection horizons and interpreted stratigraphic units. “T” refers to the transgressive ravinement discussed in the text. Location shown in Figures 5 and 7. Depth conversion assumes a velocity of 1700 m/s in sand.

Figure 12. Isopach map of modern sand deposits for the post-Sandy Fire Island West (FIW) survey; overlying contours are bathymetry in meters from the 2013 survey. See Figure 1 for location; coordinates in UTM zone 18N. Minimum detection of modern sand layer thickness is approximately 0.2 ms (~0.17 m, at 1.700 m/s). Thickness conversion assumes a velocity of 1700 m/s in sand.

Figure 13. Difference in modern sand isopach maps between the 2013 (post-Sandy) and 2011 (pre-Sandy) CHIRP surveys in the Fire Island West (FIW) region; overlying contours represent bathymetry in meters from the 2013 survey. See Figure 1 for location; coordinates in UTM zone 18N. Positive values/reddish color indicate sediment accumulation from 2011 to 2013. Heavy dashed lines trace sand ridge swales, and arrows identify preponderance of accumulation on the lee (southwest) flanks. Depth conversion assumes a velocity of 1700 m/s in sand.

Figure 14. Isopach values of mud accumulation for the post-Sandy Fire Island West (FIW) survey, overlain on the backscatter mosaic (see Figure 4). See Figure 1 for location; coordinates

in UTM zone 18N. Minimum detection of modern sand layer is approximately 0.2 ms (~0.17 m at 1700 m/s). Depth conversion assumes a velocity of 1500 m/s in soft mud. Seismic measurements of these fine-grained deposits correspond closely to the locations indicated by low backscatter values.

Figure 15. Isopach map of channel fill deposits for the post-Sandy Fire Island West (FIW) survey (see also Figure 10); overlying contours represent bathymetry in meters from the 2013 survey. See Figure 1 for location; coordinates in UTM zone 18N. Thickness conversion assumes a velocity of 1700 m/s.

Figure 16. Isopach map of modern sand deposits for the post-Sandy Fire Island East (FIE) survey; overlying contours represent bathymetry in meters from the 2013 survey. See Figure 1 for location; coordinates in UTM zone 18N. Minimum detection of modern sand layer is approximately 0.2 ms (~0.17 m at 1700 m/s). Thickness conversion assumes a velocity of 1700 m/s in sand.

Figure 17. Isopach map of channel fill deposits for the post-Sandy Fire Island East (FIE) survey; overlying contours represent bathymetry in meters from the 2013 survey. Dashed line down axis of observed channel is collocated with line in Figure 16. See Figure 1 for location; coordinates in UTM zone 18N. Thickness conversion assumes a velocity of 1700 m/s.

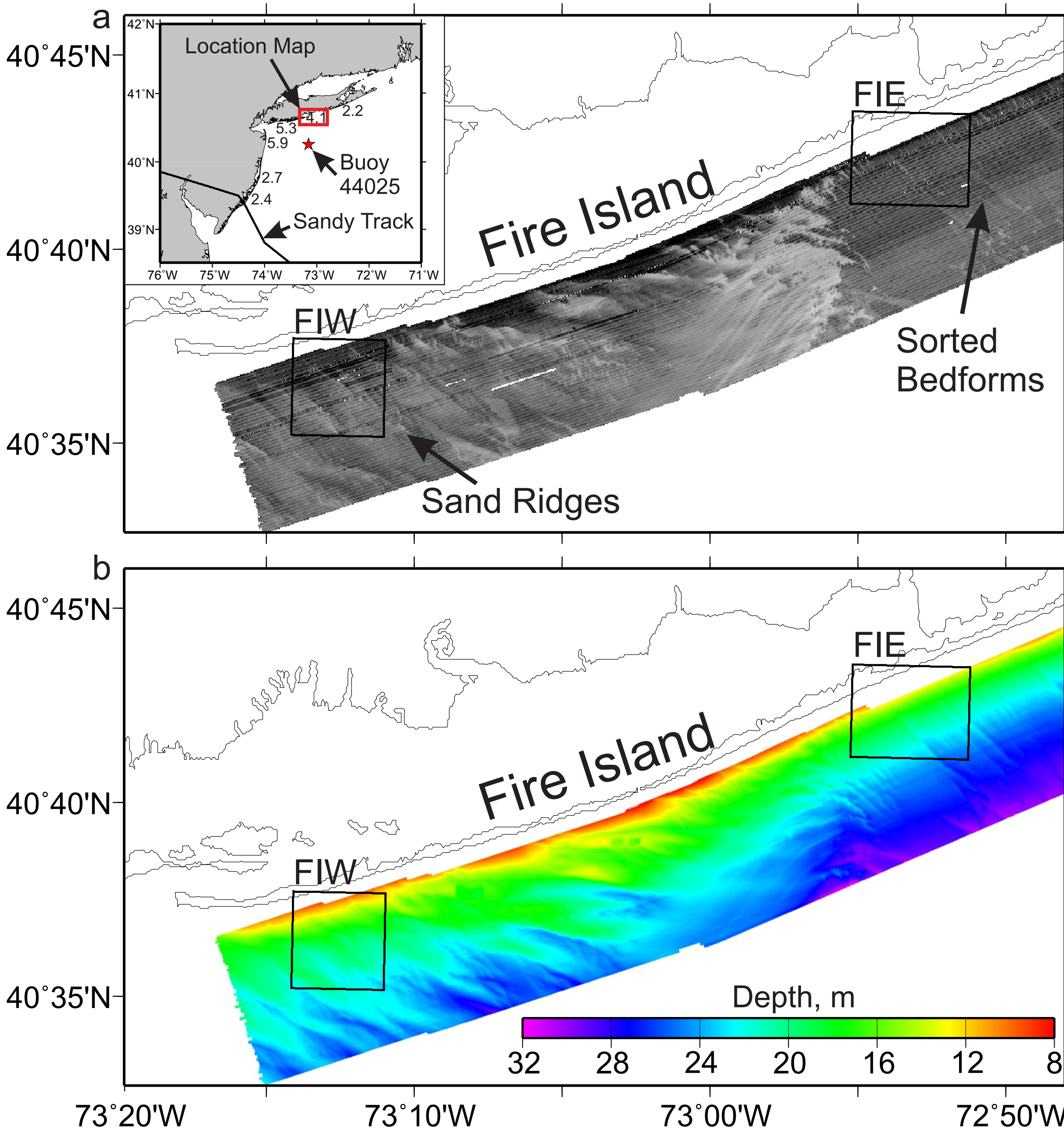

Figure 1. (a) Backscatter and (b) swath bathymetry data collected by the USGS in 2011 (Schwab et al., 2013), providing a basis for pre- and post-Sandy comparisons. Boxes indicate locations of post-Sandy Fire Island West (FIW) and Fire Island East (FIE) surveys. The FIW survey sampled sand ridges whereas the FIE survey sampled a sorted bedform morphology. Inset shows location on south shore of Long Island, the track of Sandy, location of buoy 44025 used for data plotted in Figure 2, and sampled storm tide elevations above normal along the coast in meters (USGS Portal for Hurricane Response, http://54.243.149.253/; McCallum et al., 2013).

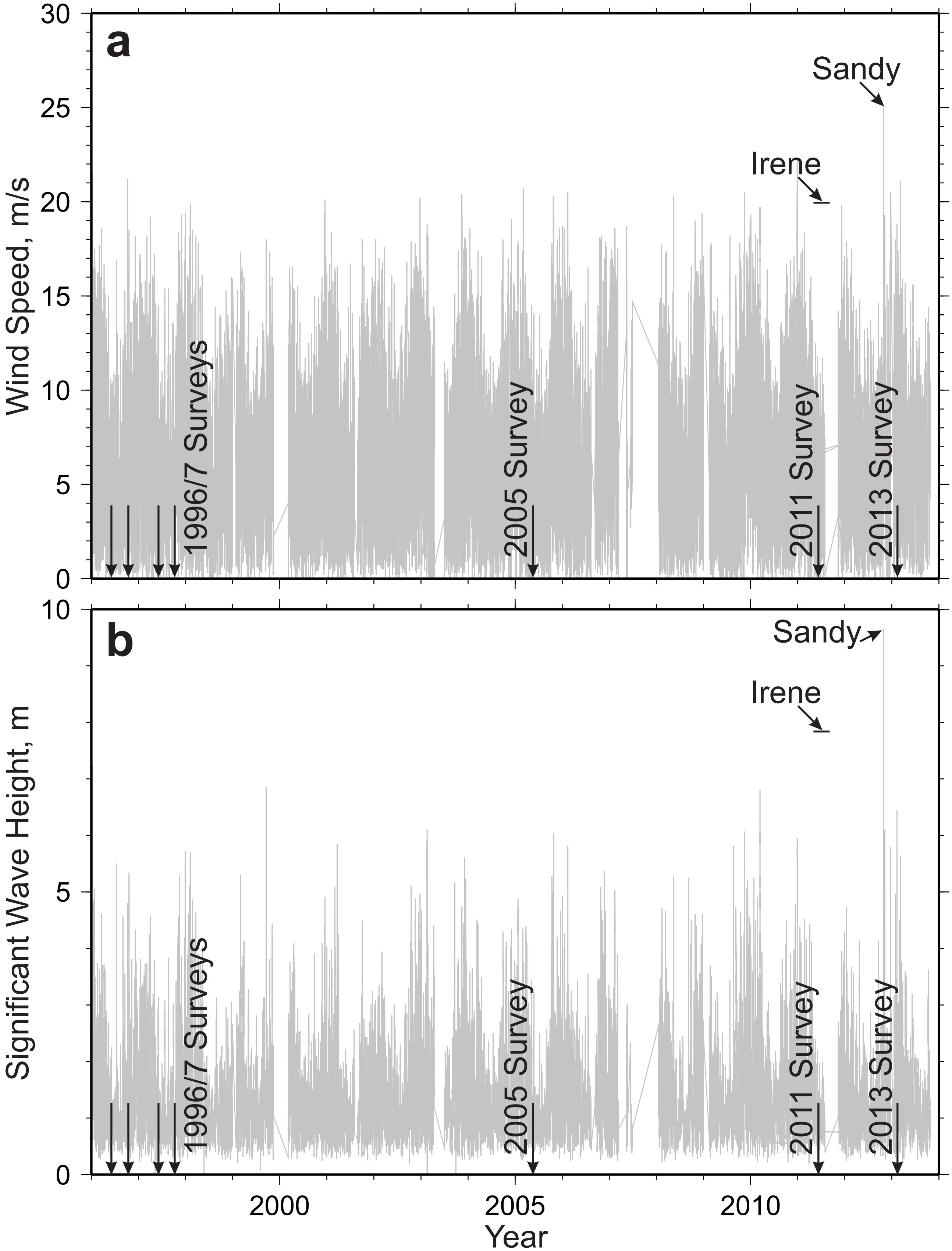

Figure 2. Sustained wind speeds (a) and significant wave heights (b) from 1996 through 2013 at NOAA buoy 44025 (http://www.ndbc.noaa.gov/station_page.php?station=44025) anchored offshore of Fire Island at ~40 m water depth (location shown in Figure 1 inset). The timing of the surveys discussed in this paper are identified. Sandy attained sustained wind speeds of 25.1 m/s and significant wave heights of 9.65 m. These values are ~25% and ~50% higher, respectively, than most other strong storms during this time period. Wave heights for Tropical Storm Irene represent the lone exception. Irene impacted the Mid Atlantic Bight in late August of 2011, after the 2011 survey and therefore within the same time window between surveys as Sandy. Buoy 44025 was not operational during this time. Peak wind and wave values for Irene are indicate from nearby buoy 44065.

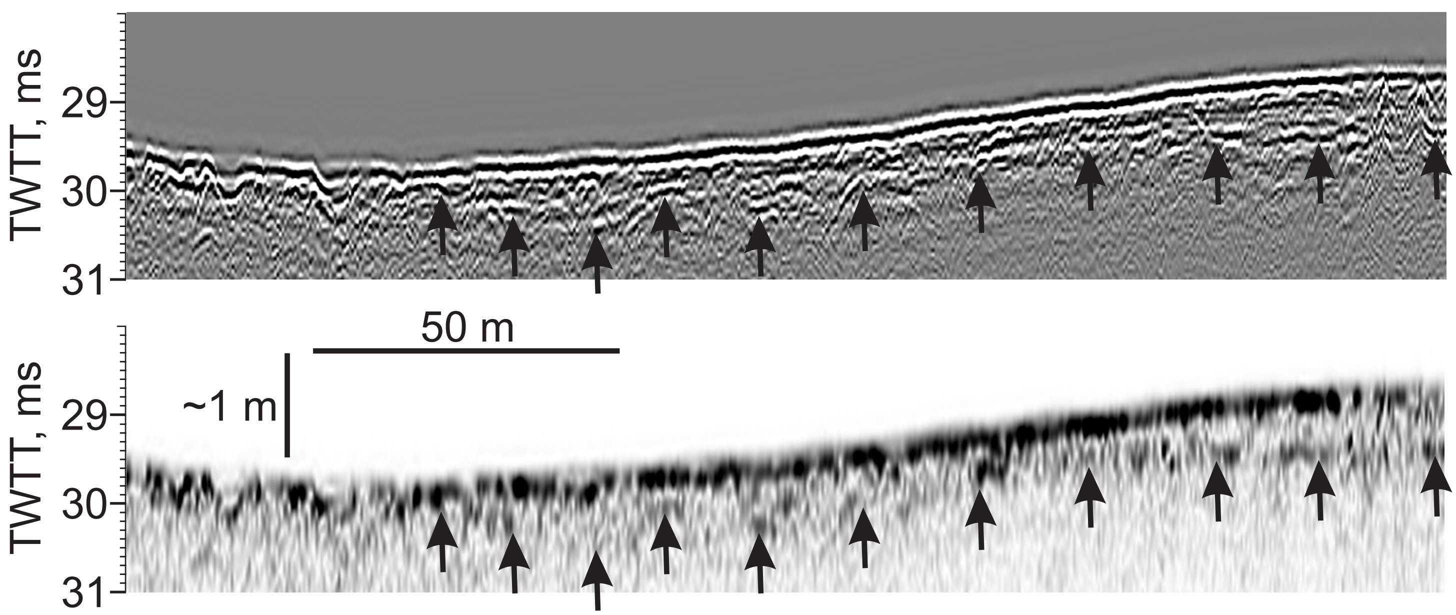

Figure 3. Example of full waveform (top) and envelope (bottom) records of CHIRP data in the FIE survey region. A shallow sub-seafloor reflection (arrows) can be confidently identified in the full waveform record, but not in the envelope record. Consequently, the former were used for interpretation and mapping of sub-seafloor horizons.

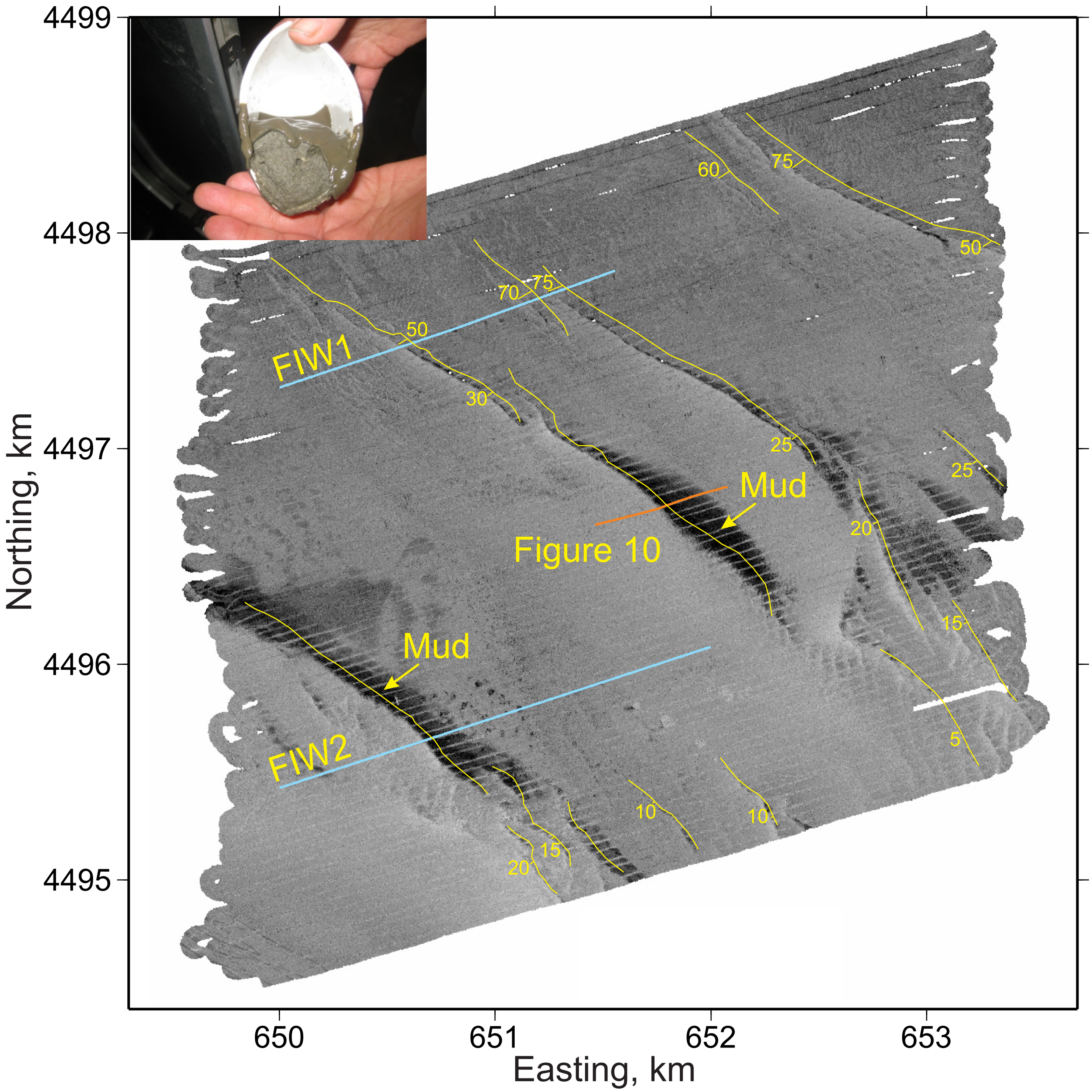

Figure 4. Post-Sandy multibeam backscatter compilation within Fire Island West (FIW) survey area; brighter shades indicate higher backscatter. See Figure 1 for location; coordinates in UTM zone 18N. Yellow lines indicate bright/dark transitions observed in 2011 backscatter data (Schwab et al., 2013). Tick marks with values indicate estimated migration of that boundary in meters between the two surveys. Inset photo shows goopy mud overlying medium sand sampled from a sediment grab in this region.

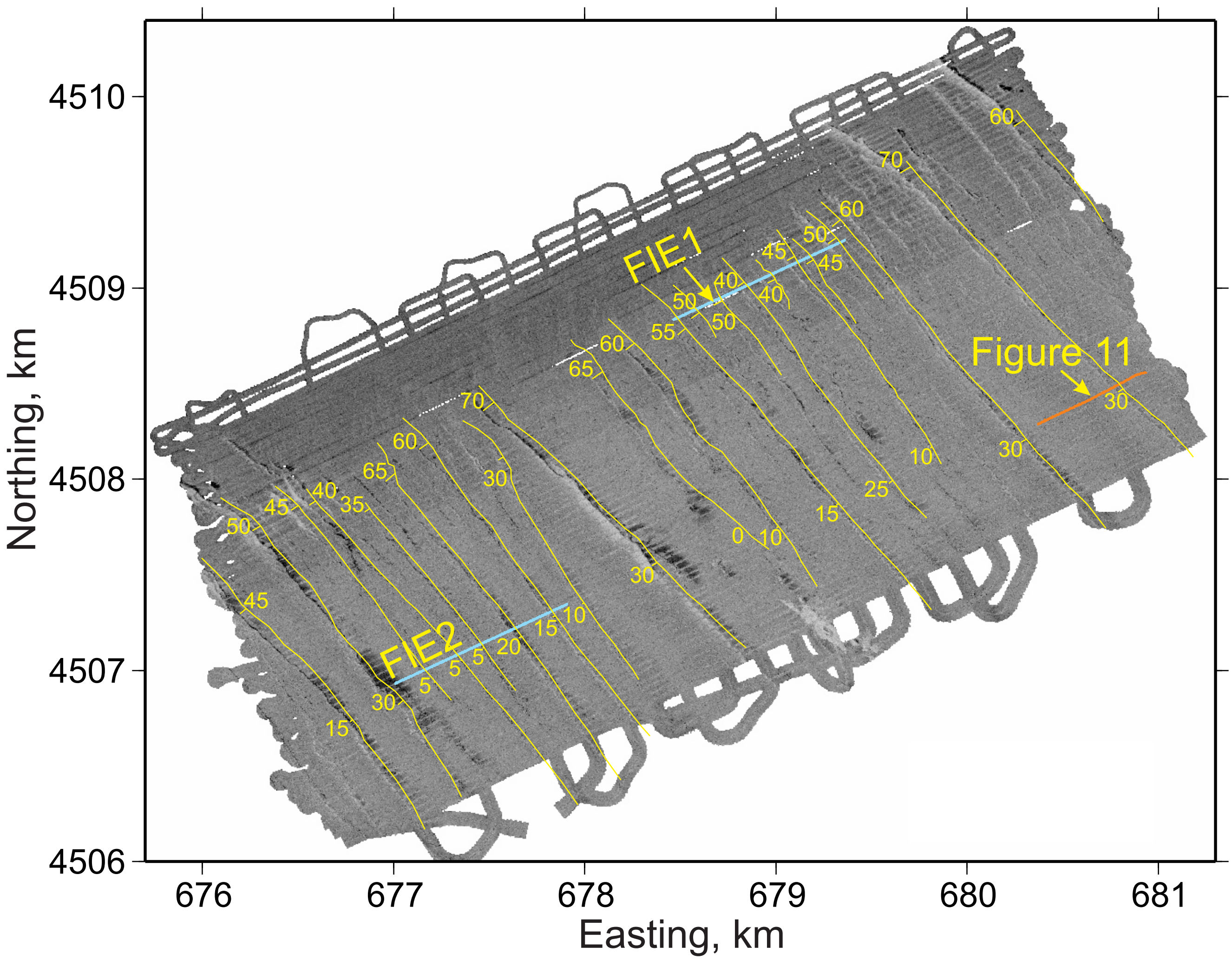

Figure 5. Post-Sandy multibeam backscatter compilation within Fire Island East (FIE) survey area; brighter shades indicate higher backscatter. See Figure 1 for location; coordinates in UTM zone 18N. Yellow lines indicate bright/dark transitions observed in 2011 backscatter data (Schwab et al., 2013). Tick marks and values indicate estimated migration of that boundary in meters between the two surveys.

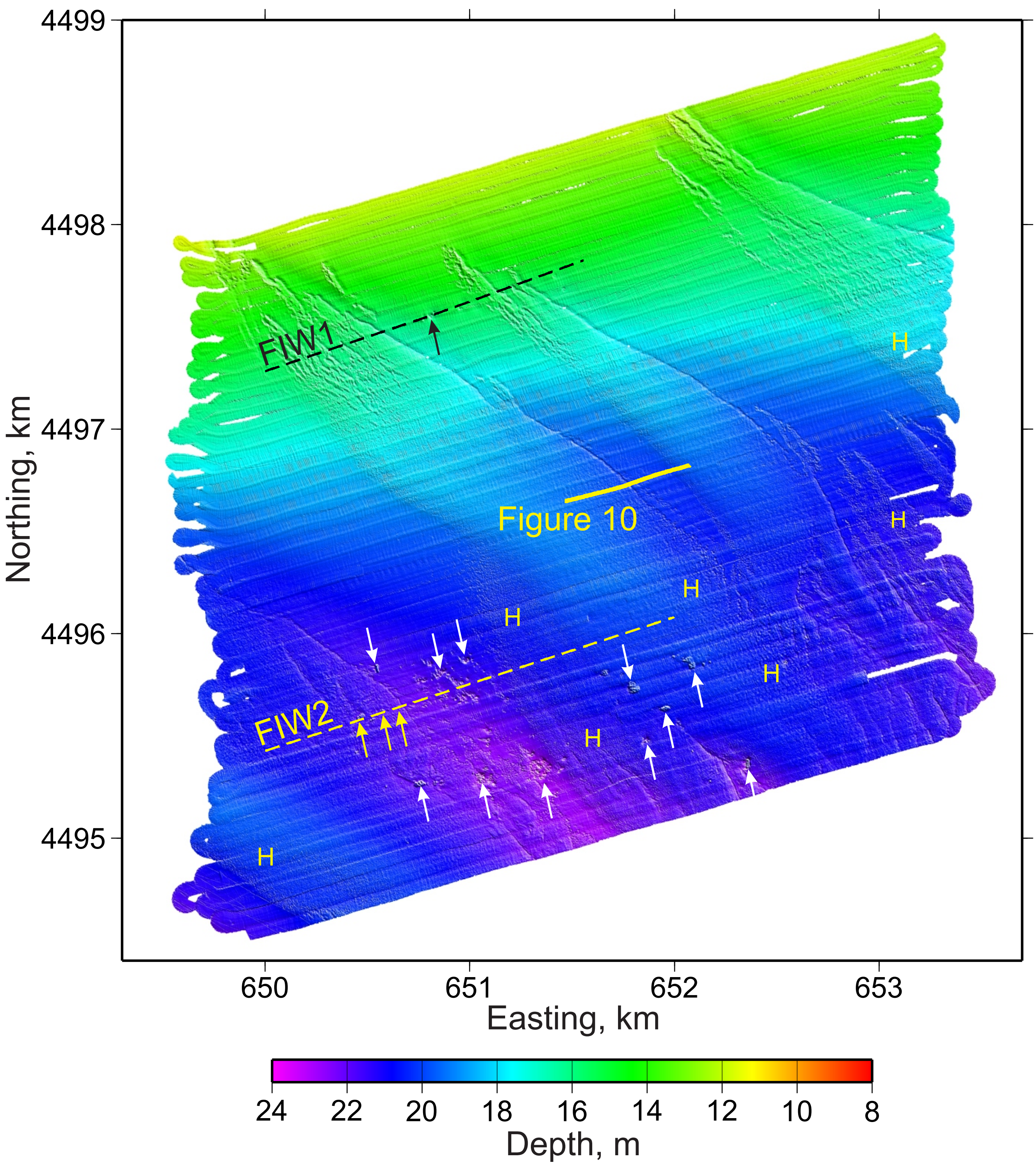

Figure 6. Post-Sandy multibeam bathymetry for Fire Island West (FIW) survey, artificially illuminated from the N. "H" highlights numerous fields of hummocky bedforms observed in the data. See Figure 1 for location; coordinates in UTM zone 18N. The black arrow indicates an object on seafloor seen on sampled profile FIW1, and the yellow arrows indicate objects on profile FIW2 (Figure 8). Numerous other artificial objects, a few of which are identified with white arrows, are observed in the south-southeast quadrant of the survey. Location is also shown for the CHIRP data shown in Figure 10.

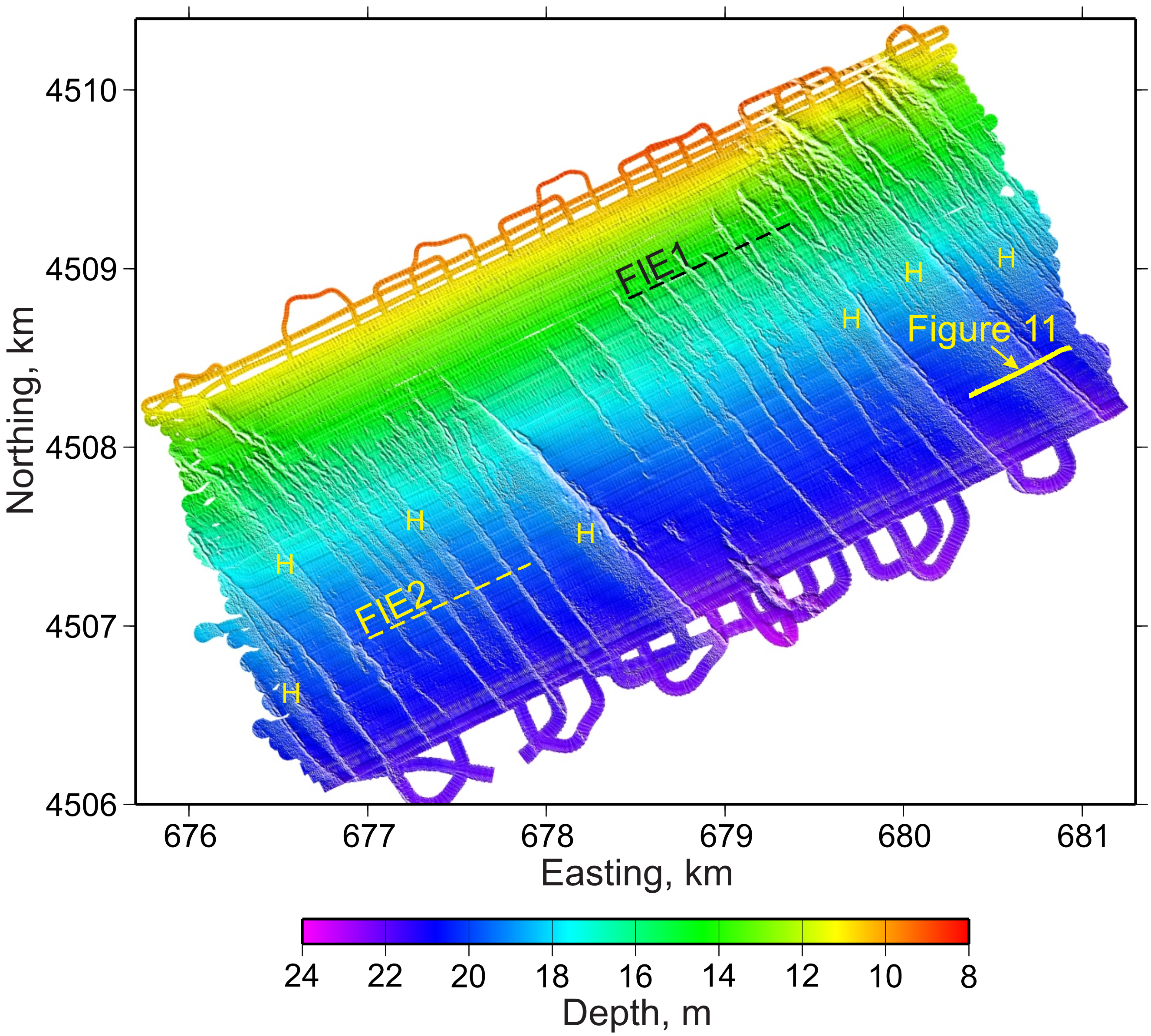

Figure 7. Post-Sandy multibeam bathymetry for Fire Island East (FIE) survey, artificially illuminated from the N. "H" highlights numerous fields of hummocky bedforms observed in the data. See Figure 1 for location; coordinates in UTM zone 18N. Profiles FIE1 and FIE2 are shown in Figure 9. Location is also shown for the CHIRP data shown in Figure 11.

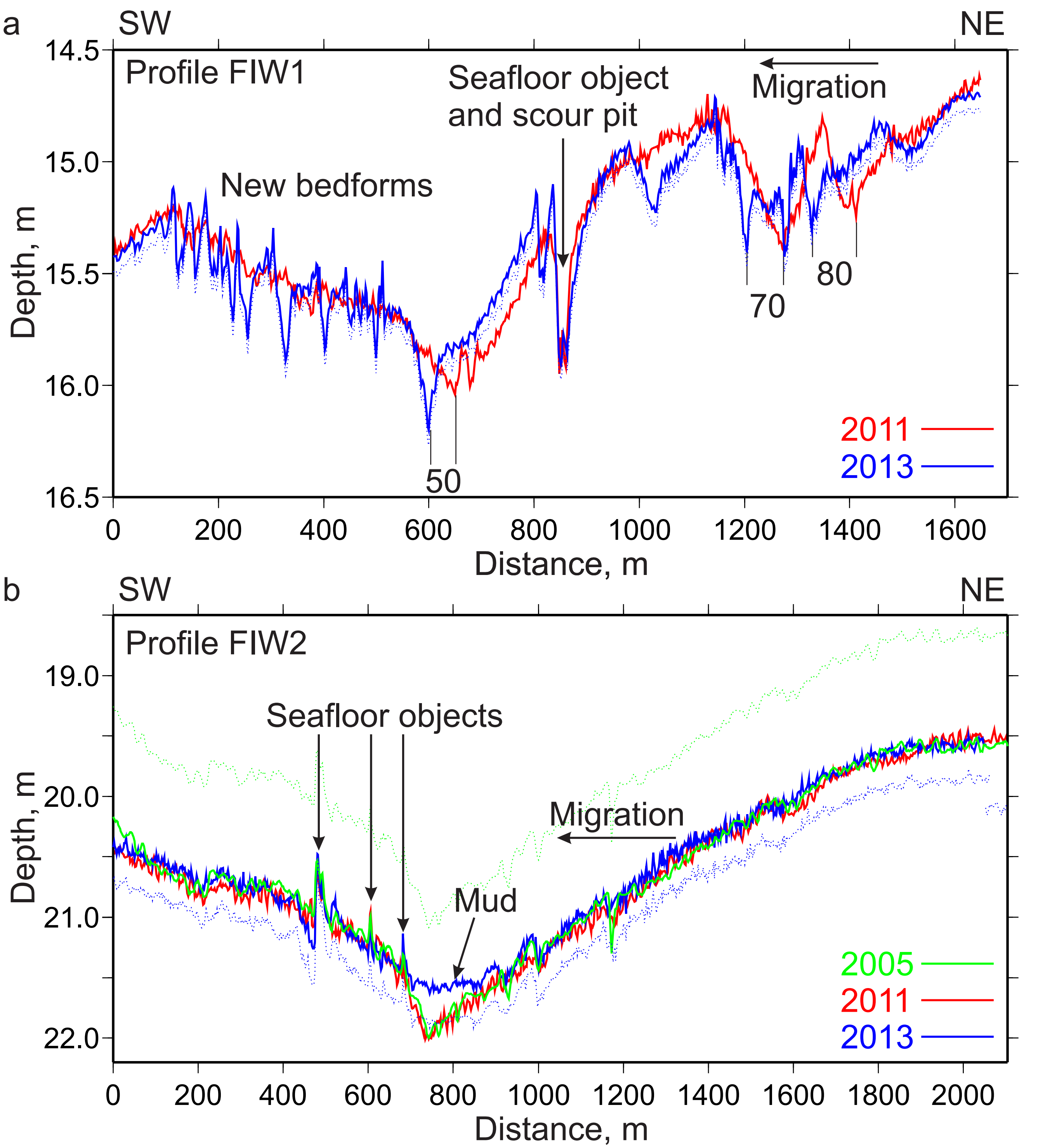

Figure 8. Comparison of bathymetry along profiles (a) FIW1 and (b) FIW2 (Figures 4 and 6) for data collected in 2005, 2011 and 2013 (post Sandy). Profiles from 2005 and 2013 were shifted to the 2011 profile vertical reference provided by emplaced seafloor objects; dotted lines of same color indicate position prior to shifting. Vertical lines and values in (a) indicate migrations of swales in meters between the 2011 and 2013 surveys. Such migration is consistently to the southwest.

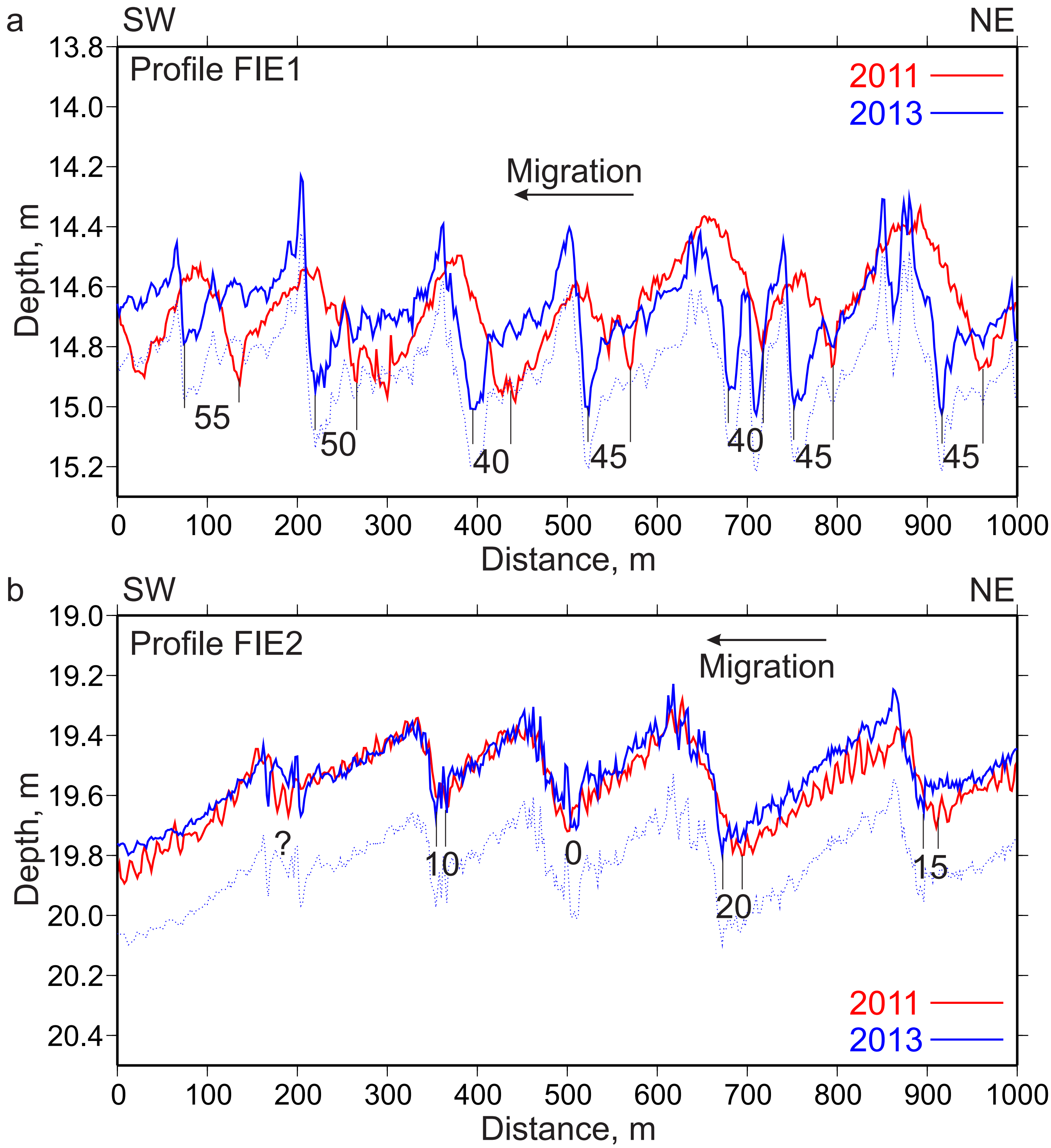

Figure 9. Comparison of bathymetry along profiles (a) FIE1 and (b) FIE2 (Figures 5 and 7) for data collected in 2011 (pre-Sandy) and 2013 (post-Sandy). Profiles from 2013 were shifted to correspond to the approximate vertical position of the 2011 profiles, but without fixed seafloor objects to provide an objective reference; dotted lines of same color indicate position prior to shifting. Vertical lines and values indicate migration of swales in meters between the 2011 and 2013 surveys. Systematic southwest migration of bedforms to the southwest is again indicated, as is true for the area of the FIW survey (Figure 8a).

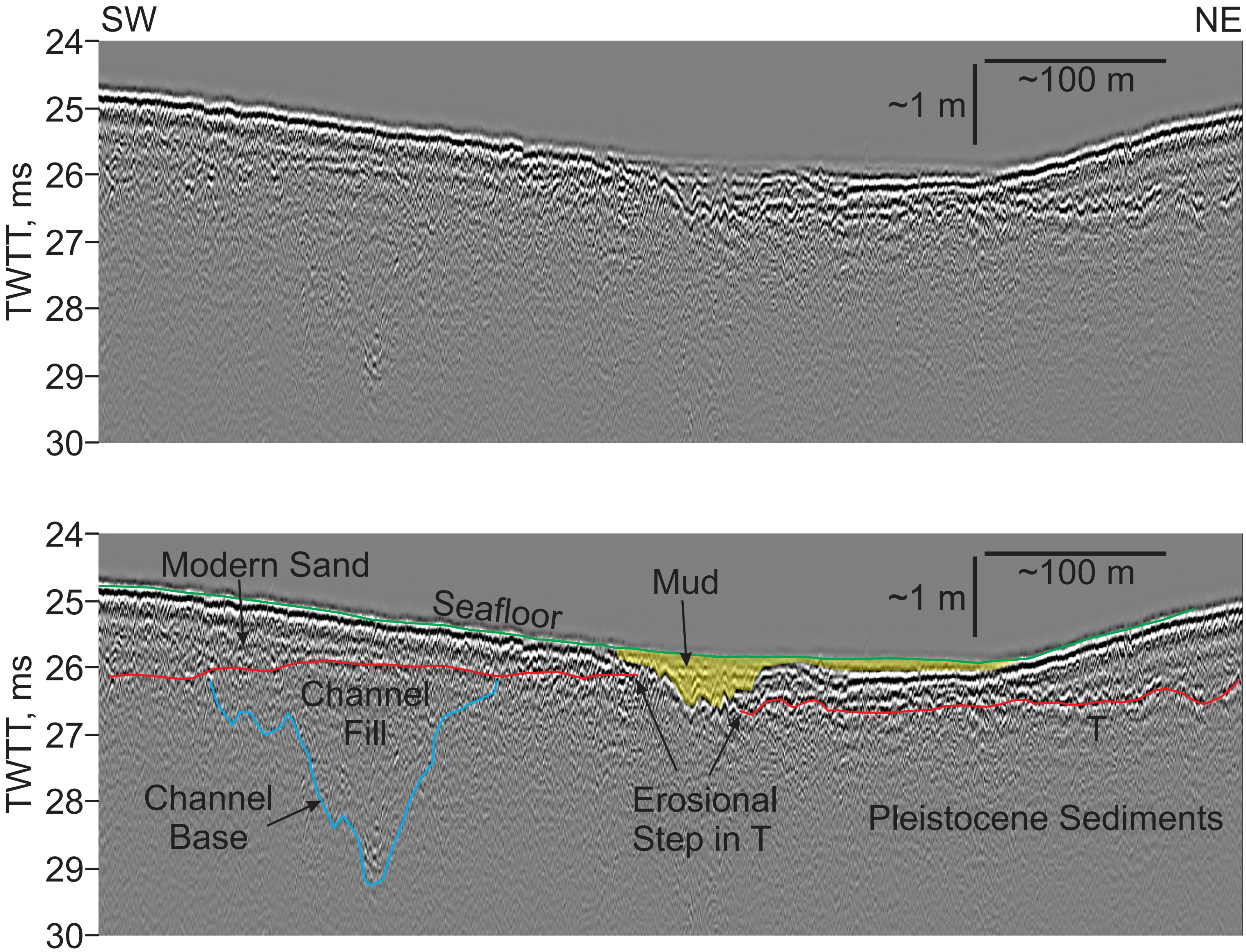

Figure 10. Uninterpreted (top) and interpreted (bottom) CHIRP acoustic reflection profile within the Fire Island West (FIW) survey area, illustrating the primary reflection horizons and interpreted stratigraphic units. “T” refers to the transgressive ravinement discussed in the text. Location shown in Figures 4 and 6. Depth conversion assumes a velocity of 1700 m/s in sand.

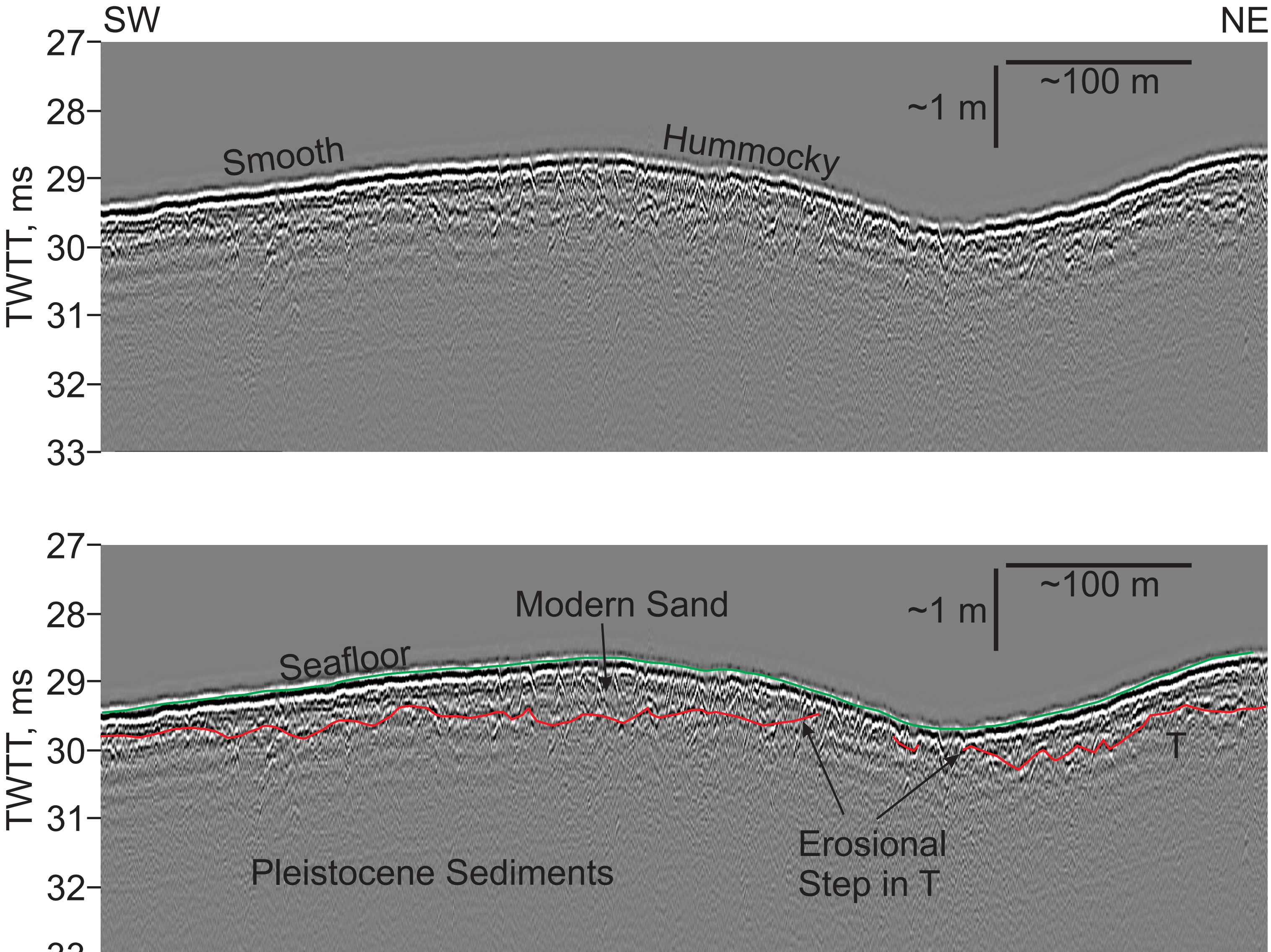

Figure 11. Uninterpreted (top) and interpreted (bottom) CHIRP acoustic reflection profile within the Fire Island East (FIE) survey area, illustrating the primary reflection horizons and interpreted stratigraphic units. "T" refers to the transgressive ravinement discussed in the text. Location shown in Figures 6 and 7. Depth conversion assumes a velocity of 1700 m/s in sand.

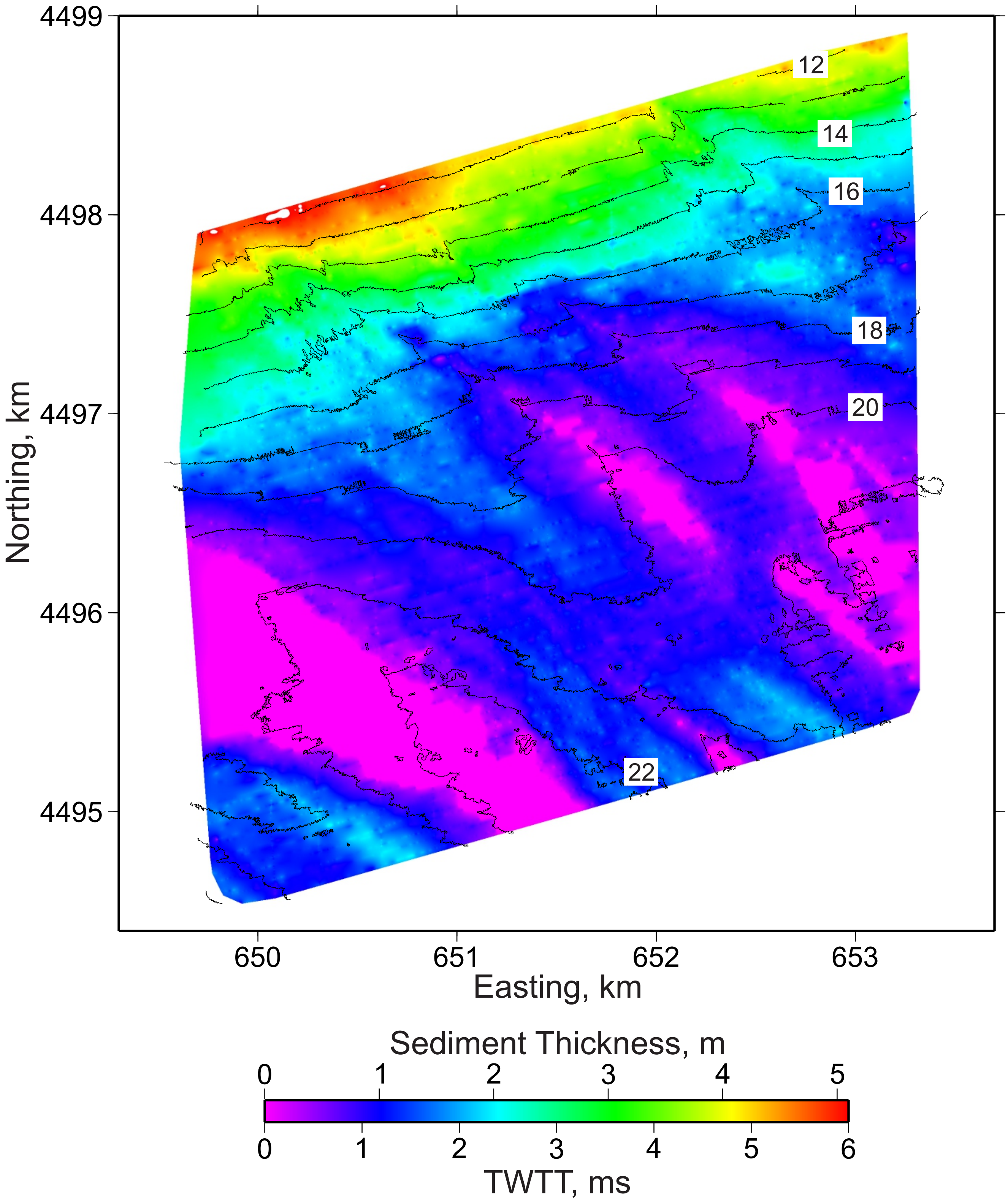

Figure 12. Isopach map of modern sand deposits for the post-Sandy Fire Island West (FIW) survey; overlying contours are bathymetry in meters. See Figure 1 for location; coordinates in UTM zone 18N. Minimum detection of modern sand layer thickness is approximately 0.2 ms (~0.17 m, at 1.700 m/s). Thickness conversion assumes a velocity of 1700 m/s in sand.

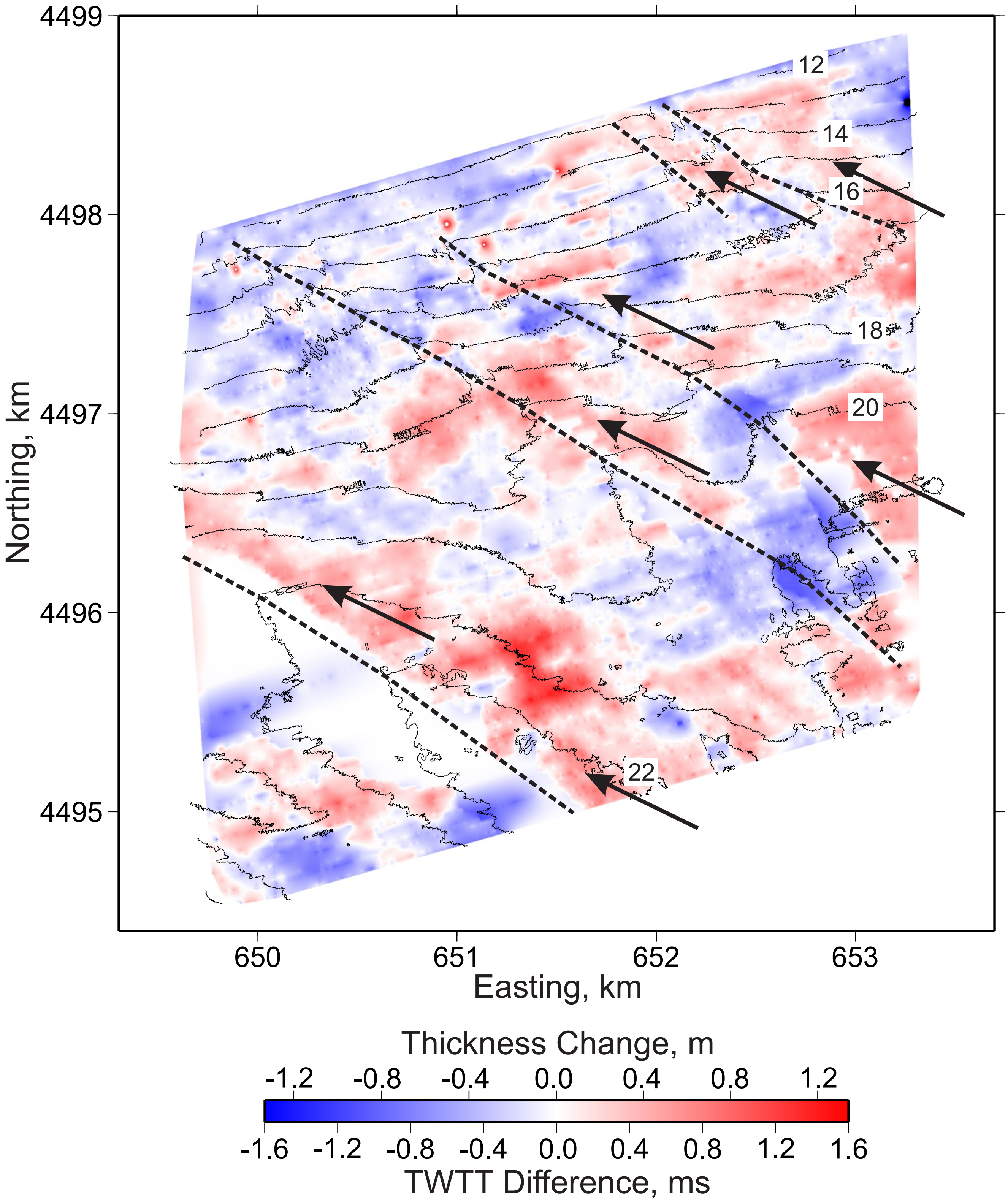

Figure 13. Difference in modern sand isopach maps between the 2013 (post-Sandy) and 2011 (pre-Sandy) CHIRP surveys in the Fire Island West (FIW) region; overlying contours represent bathymetry in meters. See Figure 1 for location; coordinates in UTM zone 18N. Positive values/reddish color indicate sediment accumulation from 2011 to 2013. Heavy dashed lines trace sand ridge swales, and arrows identify preponderance of accumulation on the lee (southwest) flanks. Depth conversion assumes a velocity of 1700 m/s in sand.

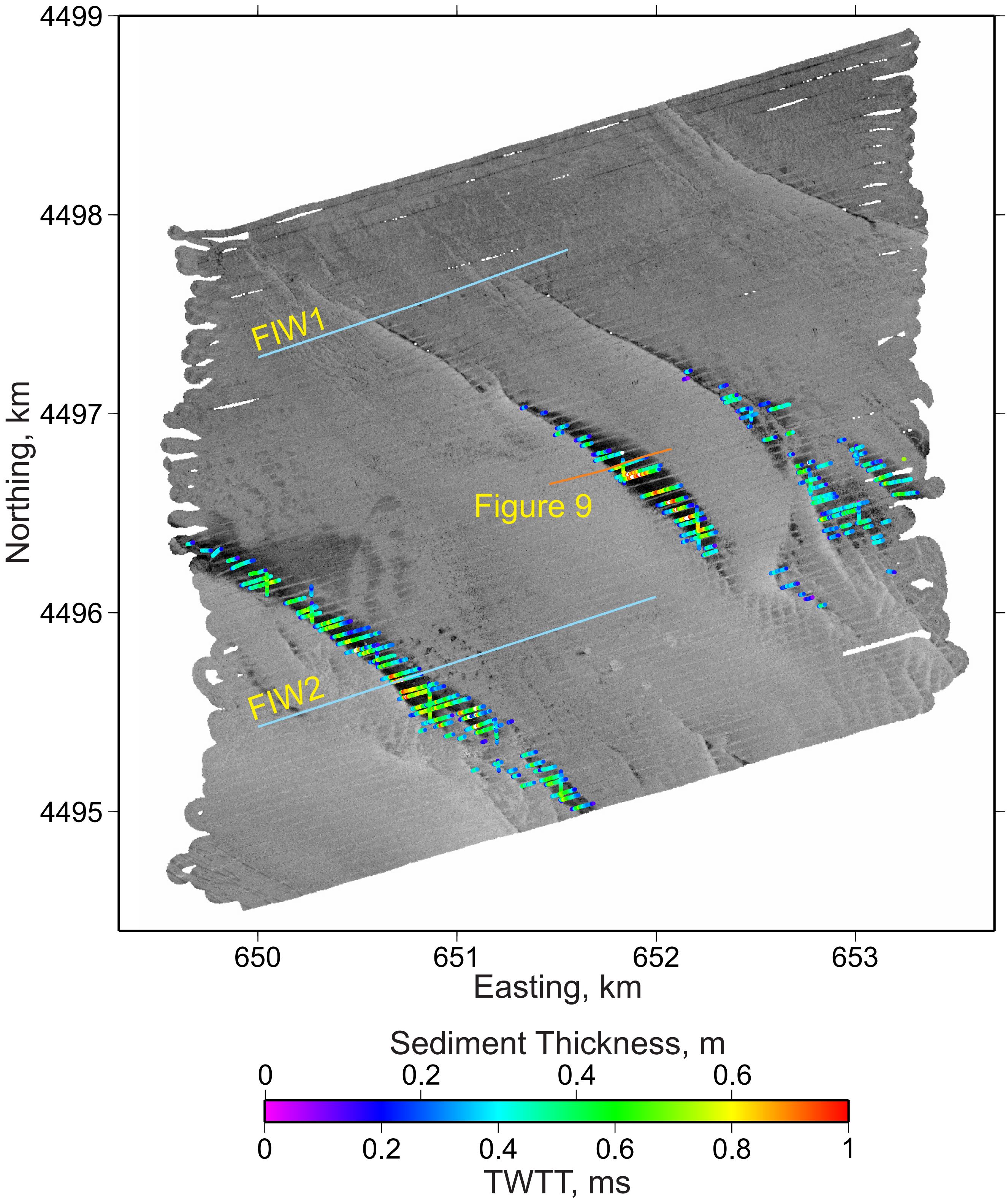

Figure 14. Isopach values of mud accumulation for the post-Sandy Fire Island West (FIW) survey, overlain on the backscatter mosaic (see Figure 4). See Figure 1 for location; coordinates in UTM zone 18N. Minimum detection of modern sand layer is approximately 0.2 ms (~0.17 m at 1700 m/s). Depth conversion assumes a velocity of 1500 m/s in soft mud. Seismic measurements of these fine-grained deposits correspond closely to the locations indicated by low backscatter values.

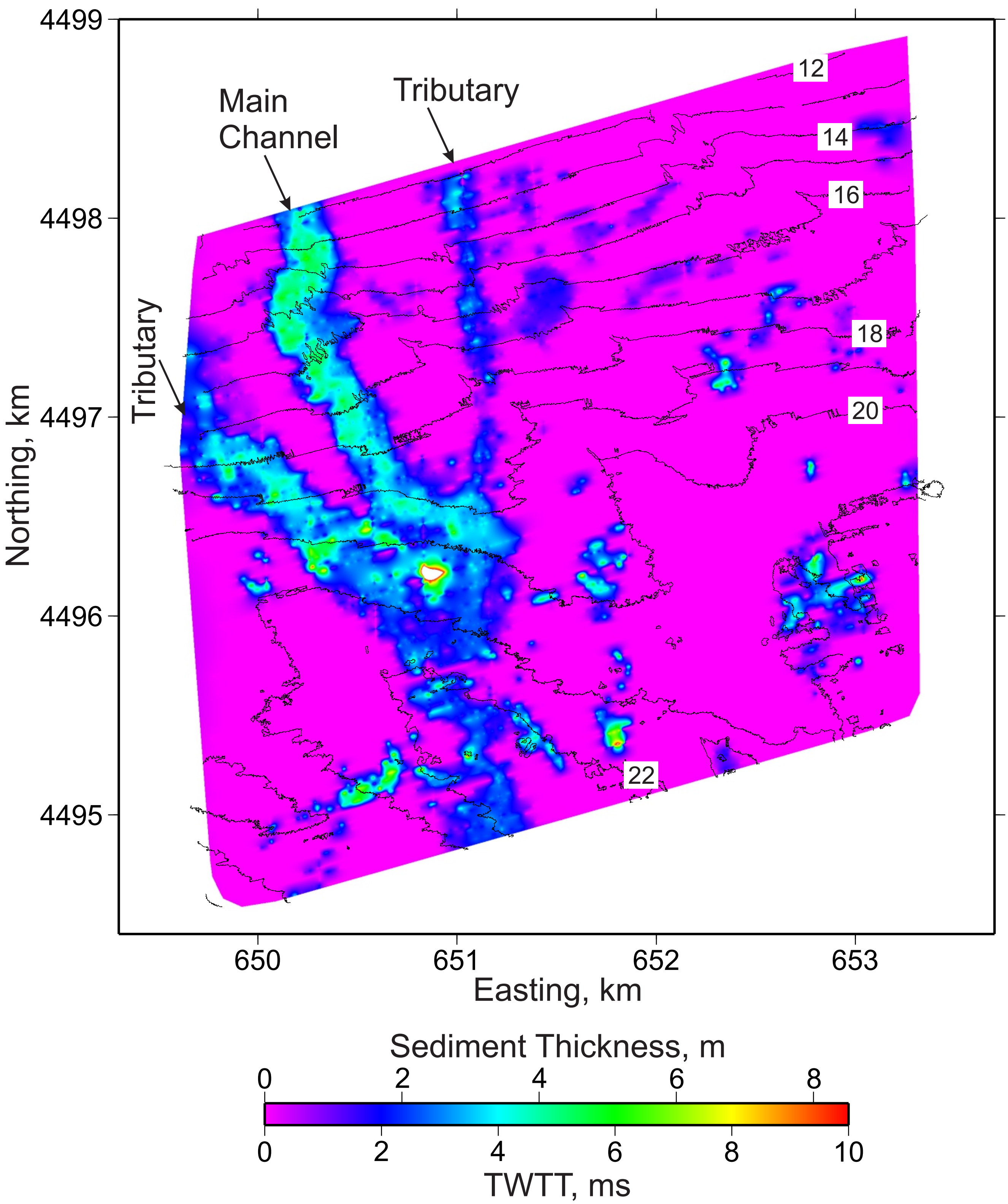

Figure 15. Isopach map of channel fill deposits for the post-Sandy Fire Island West (FIW) survey (see also Figure 10); overlying contours represent bathymetry in meters. See Figure 1 for location; coordinates in UTM zone 18N. Thickness conversion assumes a velocity of 1700 m/s.

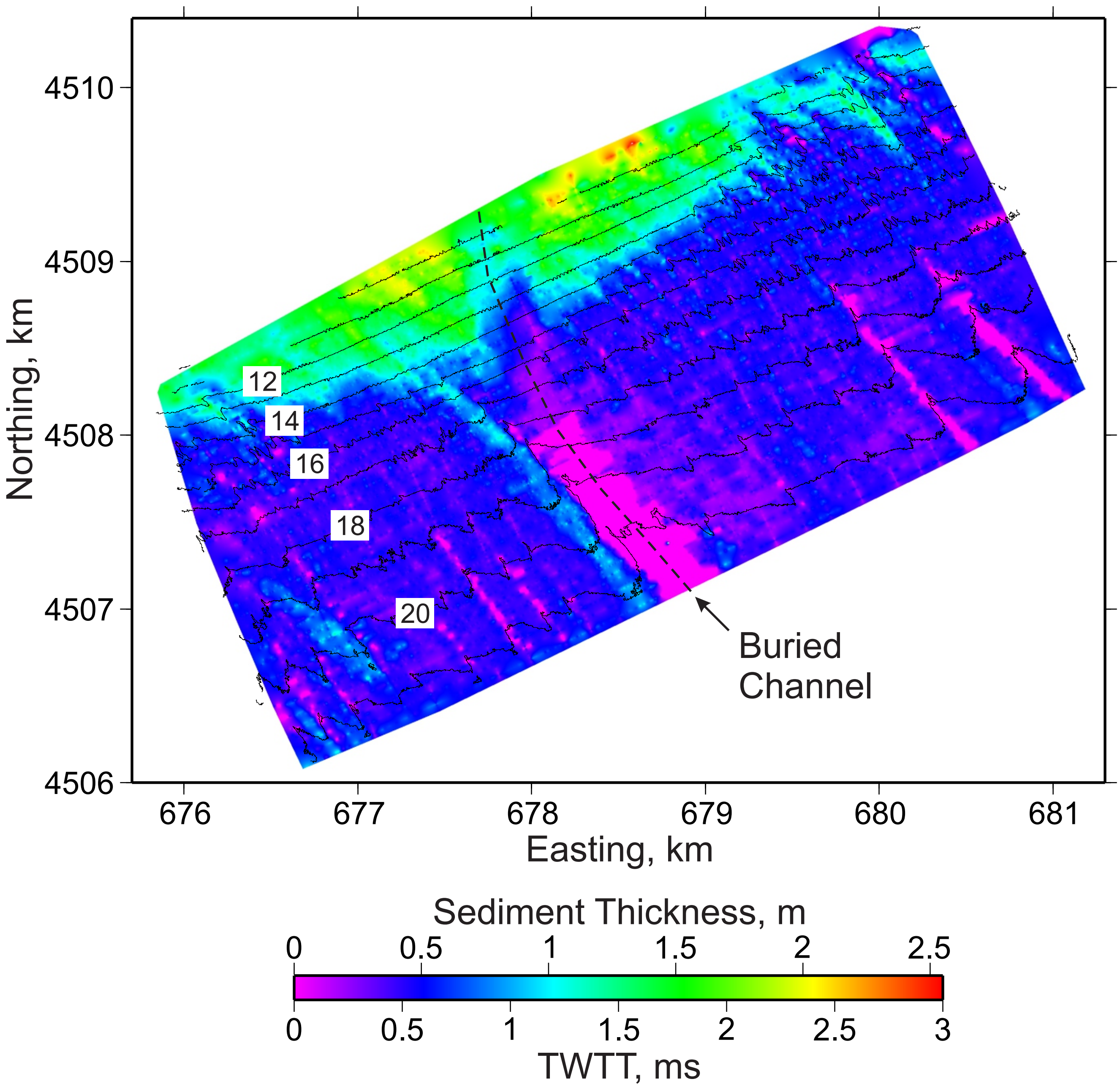

Figure 16. Isopach map of modern sand deposits for the post-Sandy Fire Island East (FIE) survey; overlying contours represent bathymetry in meters. See Figure 1 for location; coordinates in UTM zone 18N. Minimum detection of modern sand layer is approximately 0.2 ms (~0.17 m at 1700 m/s). Thickness conversion assumes a velocity of 1700 m/s in sand.

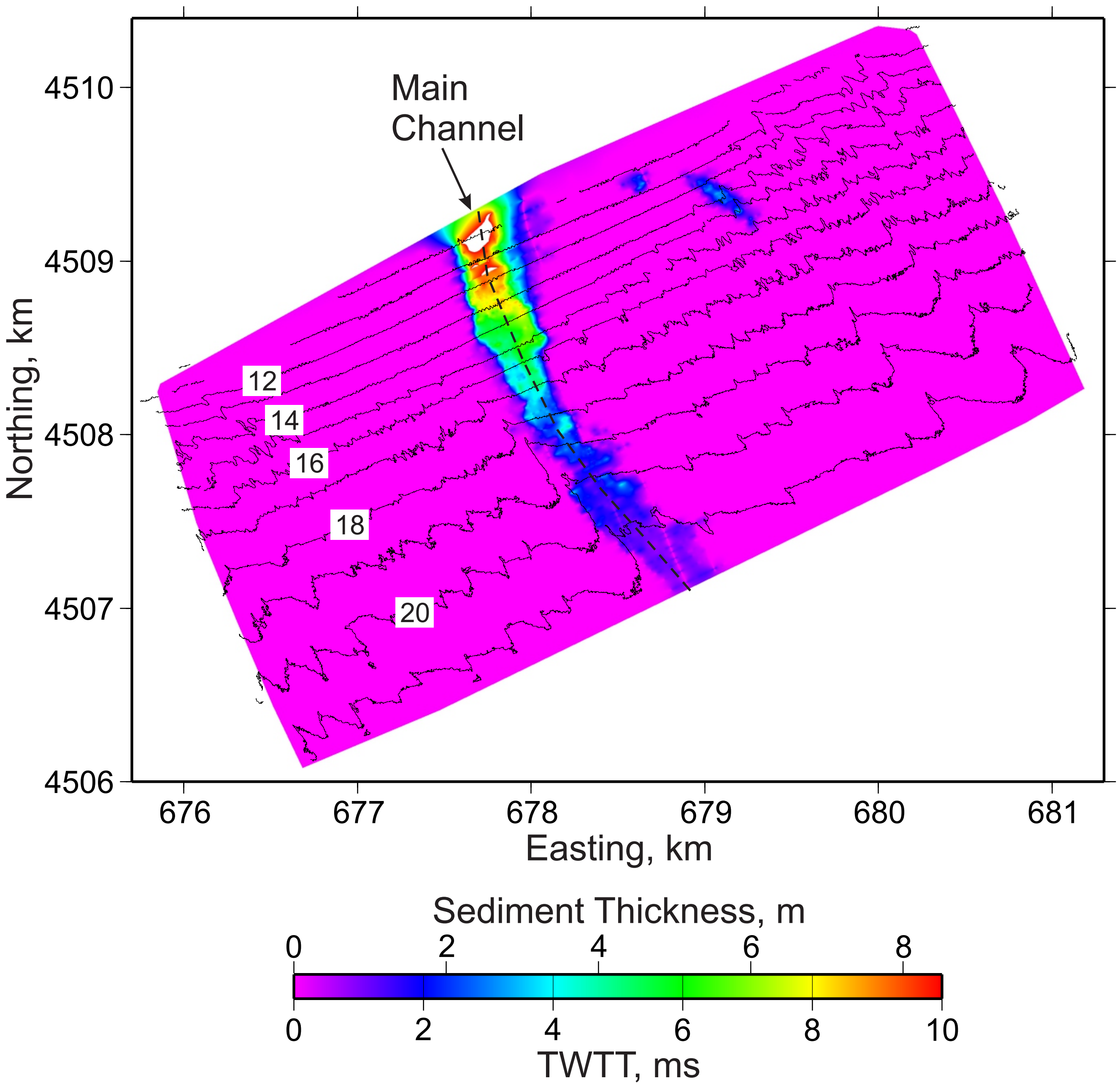

Figure 17. Isopach map of channel fill deposits for the post-Sandy Fire Island East (FIE) survey; overlying contours represent bathymetry in meters. Dashed line down axis of observed channel is collocated with line in Figure 16. See Figure 1 for location; coordinates in UTM zone 18N. Thickness conversion assumes a velocity of 1700 m/s.